UNIVERSITY OF CALIFORNIA

SANTA CRUZ

AMINO ACID STEREOCHEMISTRY AND DISTRIBUTION IN SEMI-LABILE VS REFRACTORY DISSOLVED ORGANIC MATTER: IMPLICATIONS FOR A MICROBIAL N PUMP

A thesis submitted in partial satisfaction
of the requirements for the degree of

MASTER OF SCIENCE

in

OCEAN SCIENCES

by

Amy Bour

December 2016

The Thesis of Amy Bour
is approved:

_____
Professor Matthew D. McCarthy, Chair

_____
Research Scientist Thomas P. Guilderson

_____
Professor Phoebe J. Lam

_____
Tyrus Miller
Vice Provost and Dean of Graduate Studies

TABLE OF CONTENTS

TABLES AND FIGURES

Abstract

AMINO ACID STEREOCHEMISTRY AND DISTRIBUTION IN SEMI-LABILE VS REFRACTORY DISSOLVED ORGANIC MATTER: IMPLICATIONS FOR A MICROBIAL N PUMP

by Amy Bour

Fixed nitrogen is the key limiting nutrient for primary production in much of the world ocean. While the concentration of dissolved inorganic nitrogen is below detection in open ocean subtropical gyres, micro-molar concentrations of dissolved organic nitrogen (DON) persist throughout the surface ocean. Similar to the broader dissolved organic matter (DOM) pool, the origin and molecular structure of this refractory material are largely unknown. The "microbial carbon pump" has emerged as a proposed framework for understanding microbial production of refractory DOM (R-DOM), but whether the same mechanisms also form R-DON remains unknown. Spectroscopy, radiocarbon ($\Delta^{14}C$), and concentration depth profiles of common amide-containing biomolecules together suggest that R-DON originates from proteinaceous material. Therefore, if an analogous microbial N pump exists, it most likely operates through microbial transformations of proteinaceous DON. Amino acids provide multiple potential tracers for this process, as the likely monomers contributing to amide R-DON material while their D-enantiomers (D-AAs) are unambiguous biomarkers for prokaryotic organisms.

Here, for the first time, we couple ^{14}C ages, %D-AAs, and AA molar percent abundance (Mol%) data within DOM size-reactivity fractions, in order to assess the importance of bacterial sources in the formation of R-DON. We analyzed DOM isolates representing opposite ends of the size-reactivity continuum, from surface to deep ocean in the North Pacific Subtropical Gyre. Results from this first comparison of prokaryotic contributions to DON in isolated size-reactivity fractions strongly support the idea of a microbial N pump, with higher %D in R-DOM for almost all AAs. Quantification based on mass spectral data also allowed the unambiguous

identification of three new D-AAs which had not previously been definitively identified in DOM, with oceanographically consistent depth profiles and relationships with Mol% and $\Delta^{14}C$, expanding the suite of environmentally relevant D-AAs from four to seven. Our results also suggest that several novel D-AA subgroupings could be developed as tracers: Mol% and %D trends with $\Delta^{14}C$ for Alanine (Ala) suggest that D-Ala has independent cycling mechanisms from other D-AAs, and may be strongly linked to bacterial peptidoglycan sources and cycling, while D-Leucine and D-Valine have a particularly strong relationships with $\Delta^{14}C$, with a %D maximum in the twilight zone suggesting a link to sinking particles. Interestingly, traditional degradation indices based on Mol% changes appear to indicate bacterial inputs rather than age, though we show that consistent changes in Mol% are observed with age in both DOM size-reactivity fractions as well. Overall, our results are largely consistent with the dominant production of R-DON by prokaryotic organisms, and support a greater mechanistic understanding of degradation and recalcitrance through distinct relationships between %D, Mol%, and $\Delta^{14}C$ for our expanded suite of environmentally relevant chiral AAs.

Acknowledgments

The many adventures and challenges associated with this project have been truly life changing. I am deeply grateful to my family and friends who have supported me on this journey.

None of this would have been possible without my wonderful advisor, Matt. I appreciate your phenomenal patience and insight. Thank you for giving me this chance. Thank you also to Tom, for going to extra mile to teach me about the work we did together, and Taylor, for giving me my first introduction to this field. I've learned a lot over the course of this project, and will never underestimate the significance of a stroke of luck in determining one's trajectory, or the scientific capabilities of goofy guys in Hawaiian shirts.

1. Introduction

Marine dissolved organic matter (DOM) exerts a critical influence on climate, the microbial food web, and ocean nutrient regimes. This carbon (C) reservoir is comparable in size to the atmospheric CO_2 reservoir, and equivalent to more than five years of global net primary production (Hansell et. al., 2009, Woodward, 2007, Ciais et. al., 2013). DOM likely originates almost entirely from marine primary production (Hansell et. al., 2009), however only a small fraction is identifiable as common biochemicals (Benner and Amon, 2015): despite major advances in techniques to study the DOM pool, most DOM remains structurally unidentified at the molecular level (Repeta, 2015). This is particularly true in the subsurface ocean, where DOM is characterized by "old" radiocarbon (^{14}C) ages of 4000-6000 years (Druffel et. al., 1992), and is dominated by low molecular weight compounds (Benner and Amon, 2015) with enormous diversity of molecular structures (Koch et. al., 2005).

Many explanations for the preservation of long-lived, or refractory DOM (R-DOM) have been proposed, including non-marine origin, abiotic condensation reactions, microenvironments, particle interactions, photochemistry, hydrothermal sources, and dilution (Hedges 1992, Benner and Ziegler, 1999, Nagata and Kirchman, 1999, Hedges et. al., 2000, Kirchman, 2004, Eglinton and Repeta, 2006, Ziolkowski and Druffel, 2010, Arrieta et. al., 2015, McCarthy et al., 2011). Recent work, however, has increasingly focused on microbial control of DOM cycling, with R-DOM compounds characterized by novel molecular structures and/or low concentrations, which cause metabolic costs to outweigh the benefits of biological

utilization. It has now been clearly shown that heterotrophic microbes can produce R-DOM, characterized by increased structural complexity and decreased nutrient and energy content, from simple organic molecules and common biopolymers (Ogawa et. al., 2001, Nagata et. al., 2003, Benner and Amon, 2015, Lechtenfeld, et. al., 2015). Increasing C:N elemental ratio and ^{14}C ages with decreasing molecular weight (Walker and McCarthy, 2012, Benner and Amon, 2015, Walker et al., 2016) also support bioassay data suggesting a DOM size-reactivity continuum, driven largely by heterotrophic microbial activity.

The production of R-DOM and associated C sequestration by bacteria, archaea, and viruses has recently been termed the "microbial C pump" (MCP) (Jiao et. al., 2010). For DOC, multiple mechanisms have been proposed as potentially underlying the MCP, including diversity of bacterial metabolic pathways, promiscuous ectoenzymes, and structural modification or selective remineralization associated with microbial degradation. However, the production of refractory dissolved organic nitrogen (R-DON) in many ways presents a much greater puzzle. For example, primary production, the main source of DOM, is primarily N-limited in the subtropical gyres, despite the presence of micro-molar concentrations of DON (Moore et. al., 2013, Sipler and Bronk, 2015). Though DON, like DOM, is mostly uncharacterized on the molecular level, ^{15}N-NMR analysis has indicated that DON is almost entirely in amide form (McCarthy et. al., 1997, Mao et. al. 2012, Sipler and Bronk, 2015), which strongly suggests common structures such as proteins and N-acetyl amino polysaccharides (found in peptidoglycan and chitin) as the dominant

biomolecular components (McCarthy, 1997; Aluwihare et. al., 2005). Thus, despite the ability of both phytoplankton and heterotrophic bacteria to use DON (Bronk et. al., 2007, Sipler and Bronk, 2015), and the high incentive for DON utilization to ease N-limitation, R-DON apparently persists throughout the water column, in forms resembling common biomolecules. Further, N-acetyl amino polysaccharides decrease rapidly with depth, indicating that R-DON in the deep sea is more likely peptide material (Aluwihare et. al., 2005).

Together, these observations suggest that if an analogous "microbial N pump" exists, it is manifested primarily in transformations of the proteinaceous fraction of the DOM pool. Amino acids (AAs) derived from DOM therefore likely represent the central biochemical class which can be used to investigate a potential microbial N pump at the molecular level. Like all DOM components, recoveries of identifiable AAs represent a relatively low percentage of total DON (~10-15%). Nevertheless, this yield represents by far the largest identifiable component of the DON pool (McCarthy et. al., 1996, Eglinton and Repeta, 2006). Further, the "protein-like" fraction of DOM has been ^{14}C dated to ~3000 years old in the deep North Pacific Subtropical Gyre (Loh et. al., 2004). While younger than total DOC, if correct these ages indicate that the AAs recovered via hydrolytic methods survive for multiple ocean mixing cycles, and so must represent R-DON. Together these observations suggest that chemical information about sources and mechanisms of R-DON formation are most likely locked in the AA pool.

Fortunately, the structural diversity of AAs provides a wealth of molecular tracer potential. Source, relative degradation state, and recalcitrance of proteinaceous materials have all been assessed using several different indicators, including AA stereochemistry and molar percent abundance-based metrics (Dauwe et. al., 1999, Yamashita and Tanoue, 2003, McCarthy et. al., 2004, Lechtenfeld et. al., 2015). Among these multiple proxies, D-AAs are uniquely powerful tracers for bacterial source and transformation. The synthesis and incorporation of the D-enantiomers of AAs (D-AAs) are unique to prokaryotic organisms, allowing AA stereochemistry to be used as an indication of microbial activity in environmental samples (Radkov and Moe, 2014). The MCP framework potentially connects D-AAs to DOM recalcitrance, with D-AA abundance providing an additional, source-specific AA-based metric to compliment the more traditional degradation index (DI, Dauwe et. al. 1999).

Here we use a novel approach coupling $\Delta^{14}C$ data with %D-AAs and AA-Mol% in independently isolated HMW- and LMW-DOM, to directly test ideas about importance of bacterial sources in the formation of R-DON. We also compare assessments of degradation and recalcitrance based on these same metrics in a sample set representing opposite ends of the DOM size-reactivity continuum, from surface to deep waters of the North Pacific Subtropical Gyre. We evaluate a potential "microbial N pump," by analyzing AA enantiomers and molar percent abundance distributions in the context of $\Delta^{14}C$ ages for semi-labile (SL-) vs. R-DOM isolates. Our results are largely consistent with the dominant production of R-DON by prokaryotic organisms, and substantially broaden the suite of D-AAs previously

confirmed in the DOM pool. At the same time, we also observed important differences in relationships between D-AAs, molecular weight fraction, DI, and $\Delta^{14}C$, indicating that these metrics track different aspects of degradation. In particular, independent trends for individual AAs suggest D-AA subgroupings may also have unique tracer potential for specific bacterial sources, and potentially allow the first mechanistically grounded DI formulation for DOM.

2. Experimental Methods

2.1. Experimental Design and Water Sampling

Our experimental framework was designed to test the microbial N pump hypothesis by comparing AA enantiomers and ^{14}C in isolated HMW- and LMW-DOM in a depth profile in the North Pacific Subtropical Gyre. We used a sequential sampling approach, first isolating the HMW-DOM using a large-volume tangential-flow ultrafiltration (UF) system, then isolating the remaining LMW-DOM from the UF permeate by solid-phase extraction (SPE) (Fig. 1). A detailed description of the development of this sampling protocol are presented elsewhere (Broek et al., 2016; Broek et al., in prep.). Briefly, sampling was conducted at Hawaii Ocean Time Series Station ALOHA (A Long-Term Oligotrophic Habitat Assessment; 22°45'N, 158° 00'W) aboard R/V Kilo Moana cruises KM 14-18 (August-September 2014) and KM 15-06 (May 2015). Significant extra precautions were taken to ensure ^{14}C-tracer free shipboard sampling, including ^{14}C swabs to identify areas potentially exposed to ^{14}C tracer, and preparation of lab spaces by floor-to-ceiling cleaning with 10% HCl

followed by ethanol, and construction of a plastic sheeting "bubble" (Broek et al., 2016; Broek et al., in prep).

Water samples from 400, 850, and 2500 m were collected by repeated casts of a 24-bottle rosette of 12 L Niskin bottles, drained through platinum cured silicone tubing to acid washed (10% HCl) and sample rinsed fluorinated high density polyethylene (F-HDPE) carboys, which were subsequently emptied into acid washed 1000 L HDPE containers for storage, lasting no more than 12 hours. Surface water was sampled via the vessel's underway sampling system, with intake on the bow of the vessel at approximately 6 m depth. The flow-through system was flushed for 2 hours prior to surface sampling. Seawater from each depth was pre-filtered through 53 μm Nitex mesh, and pumped through a 0.2 μm polyethersulfone (PES) cartridge filter (Shelco Filters, Micro Vantage, water grade, 9.75" DOE, polycarbonate housing) before UF. The total water volume per depth was 3000-4300 L.

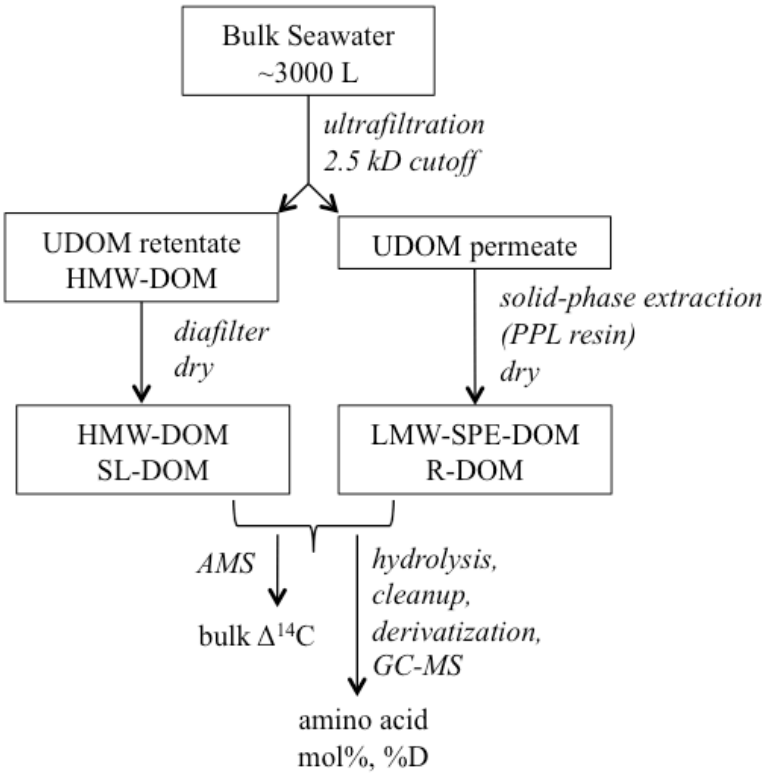

Figure 1. Experimental Design. Large-volume isolations of HMW- and LMW-SPE-DOM were performed by sequential extraction of HMW-DOM by ultrafiltration, followed by solid-phase extraction of the remaining LMW-DOM from the ultrafiltration permeate (see Broek et. al. 2016, Broek et. al., in prep.). Depth profiles including surface, 400, 850, and 2500 m were sampled in August-September 2014 and May 2015 at Station ALOHA (22°45'N, 158°00'W). To examine the relationship between age and bacterial biomarkers (D-AAs), bulk $\Delta^{14}C$ was measured by accelerator mass spectrometry, and AA Mol% and enantiomeric ratios were measured by GC-MS.

2.2. Coupled Tangential-Flow Ultrafiltration and Solid-Phase Extraction

The main UF system was constructed using a modified design of the system described by Roland and coauthors (2009), and expanded on by Walker and coauthors (2011), using four-spiral wound PES UF membranes (GE Osmonics GH2540F30, 40-inch long, 2.5-inch diameter, 2.5 kD MWCO) to isolate HMW-DOM (2.5 kD-0.2 μm) (Broek et. al., in prep.). The final retentates were collected in 15-20 L volumes, and transferred to a reconfigured, smaller-volume system, where they were further reduced to 2-3 L, and then diafiltered with 40 L of 18.2 MΩ Milli-Q water using a single UF membrane (GE Osmonics GE2540F30, 40-inch long, 2.5-inch diameter, 1 kD MWCO) to remove salts (Broek et. al., in prep.).

UF permeate was collected in acid-cleaned 200 L HDPE barrels and acidified to pH 2 for solid-phase extraction of LMW-DOM. SPE procedures follow those of Dittmar and coauthors (2008), loading no more than 10L seawater/1g Agilent PPL sorbent (Broek et. al., in prep.). Following sample loading, the SPE sorbent was desalted by flushing with 6 L of pH 2 MQ water, and eluted with five to six 500 mL additions of methanol (MeOH). Eluted MeOH solution was stored in pre-combusted amber glass bottles at -20°C for transport.

In the laboratory, HMW- and LMW-SPE DOM were further concentrated by rotary evaporation (rotavap), at 30 inHg vacuum at 45°C for HMW-DOM, and 22.5 inHg at 30°C for LMW-SPE-DOM, with 0°C condenser. All rotovap glassware was pre-combusted (450 °C, 5 h), and a sequential in-line combination of molecular sieve material and a liquid nitrogen trap were paced between the vacuum pump and rotovap

chamber to ensure no contamination of isolated material from back streaming of hydrocarbons or other contaminants. After reduction to 50-100 mL, samples were transferred to acid and solvent cleaned polytetrafluoroethylene (PTFE) centrifuge tubes, and dried to powder in a Jouan centrifugal evaporator (Societe Jouan, Saint-Herblain, France) at a chamber temperature of 55 °C. Dry material was transferred to pre-combusted glass vials and stored in a desiccation cabinet until $\Delta^{14}C$ and AA enantiomeric analysis.

2.3. $\Delta^{14}C$ Analysis

Relationships between MW and age for the DOM fractions were confirmed by bulk $\Delta^{14}C$ measurements at the Center for Accelerator Mass Spectrometry at Lawrence Livermore National Lab. Aliquots of each DOM sample were transferred into pre-combusted quartz tubes, amended with pre-combusted cupric oxide and silver, and flame sealed under vacuum. Combustion and graphitization procedures followed Vogel et. al. (1984). Fraction modern values were determined following the conventions set forth by Stuiver and Polach (1977) with the Libby half-life of 5568 years. Corrections were applied for mass-dependent fractionation using the sample $\delta^{13}C$ value, and for background (scaled to sample size) based on measurements of ^{14}C-free humic acid. Reported $\Delta^{14}C$ values are corrected for sampling year.

2.4. Sample Preparation for Analysis of Amino Acid Enantiomers

Liquid hydrolysis was selected as the best method to release AAs while minimizing the racemization blank (Kaiser and Benner, 2005). Aliquots of 3.75 mg C for each HMW-DOM and LMW-SPE-DOM sample were weighed into combusted

vials (450°C/5 hrs), and combined with 3 mL 6 M HCl. Vials were purged with N_2, and heated to 110°C for 20 hr. HCl was removed under a stream of N_2, and the hydrolysates were re-dissolved in 1 mL of 0.1 M HCl. Hydrolysates were purified using cation-exchange chromatography (Bio-Rad AG50W-X8, 200-400 mesh), following the methods of Takano et. al. (2010). Ammonium hydroxide was removed using the Jouan centrifugal evaporator (Societe Jouan, Saint-Herblain, France) at a chamber temperature of 55 °C, and samples were re-protonated by dissolving in 1 mL 0.1 M HCl. Trifluoroacetyl isopropyl ester derivatives were prepared using the protocol of Silfer et. al. (1991), with some modifications (Décima et. al., 2013). AAs were further purified by solvent extraction followed by re-acetylation, as described by Décima et. al. (2013). Samples were stored at -20°C for up to two weeks before analysis. Immediately before analysis, cold samples were dried under a N_2 stream and re-dissolved in ethyl acetate.

2.5. GC-MS Analysis and Quantification

AA enantiomers were analyzed using a GC-MS (Agilent 7890A + 5975B) equipped with a chiral column (Altech Chirasi-L-Val, 50 m length, 0.25 mm internal diameter, 0.16 μm film thickness). 1 μL of sample was injected through a splitless inlet at 200°C, with helium carrier gas flowing at 0.9 mL/min. The oven program for each 57.5 min run was as follows: Starting at 45°C, increase 2°C/min to reach 75°C. Then increase at 4°C/min to reach 110°C. Continue to heat at 1°C/min to reach 125°C, then heat at 4°C/min to reach 200°C. Quantification was based on peak areas obtained using single-ion monitoring, with the following characteristic ion fragments

(m/z): Alanine (Ala), 140; valine (Val), 168.1; threonine (Thr), 153; glycine (Gly), 126; isoleucine and leucine (Ile and Leu), 182.1; serine (Ser), 138; proline (Pro), 166.1; aspartic acid (Asp), 184; glutamic acid (Glu), 180; and phenylalanine (Phe), 190.1.

Amino acid yields were quantified using mixed L-AA standards in a linear four-point calibration curve ranging from 1-1000 μmol/AA. For each AA, peak areas for both enantiomers were converted to picomoles using the calibration curve for the corresponding ion fragment. All standards were added to the sample preparation stream at the derivatization step. Recoveries of individual AA enantiomers in samples ranged from 1 pmol-1.2 nmol.

2.6. Data Analysis

2.6.1. %D Amino Acids and Racemization Correction

Quantification of AA enantiomers requires corrections for racemization during sample preparation (Kaiser and Benner, 2005). This occurs when the samples are heated during hydrolysis and derivatization. Hydrolysis racemization blanks are the average %D of those determined by Kaiser and Benner (2005) for free AAs and proteins; the uncertainty in the hydrolysis racemization is the standard deviation of the population defined by the greatest hydrolysis racemization of the AA in a protein, and the least hydrolysis racemization of the free AA. Derivatization racemization is the average %D measured in four small L-AA standards (3 pmol/AA) added to the sample preparation stream at the derivatization step. The uncertainty in the derivatization racemization is the sample standard deviation of these values.

The total racemization blank is the sum of the hydrolysis and racemization blanks, and the racemization-corrected picomoles of L-AAs were calculated as described by Kaiser and Benner (2005):

$$L_0 = \frac{L_m - D_m\left(\frac{D}{L}\right)_b}{1-\left(\frac{D}{L}\right)_b}$$

where L_0 is the original concentration of the L-enantiomer, L_m and D_m are the measured concentrations of the enantiomers, and $(D/L)_b$ is the enantiomeric ratio in the blank: $D/L=\%D(100-\%D)^{-1}$. Reported errors represent ±1 standard deviation in the propagated uncertainty in the racemization blank. After racemization correction, %D is defined as

$$\%D = 100 \times \left(\frac{D_0}{D_0 + L_0}\right) = 100 \times \left(\frac{D_0}{D_m + L_m}\right)$$

where D_0, the original concentration of the D-enantiomer, is determined based on the relationship $L_m+D_m= L_0+D_0$.

2.6.2. Amino Acid Molar Percent Abundance Calculation

For each AA, the molar percent abundance (Mol%) was calculated using the sum of the D and L enantiomers. For a given AA_i, Mol%-AA_i is defined as

$$Mol\% - AA_i = \frac{pmol\ AA_i}{total\ pmol\ AAs}$$

where total pmol AAs includes both enantiomers of Ala, Asp, Glu, Ser, Leu, Val, Phe, Gly, Pro, Ile, and Thr.

2.6.3. Degradation Index calculation

The degradation index (DI) was calculated using the classic formulation proposed by Dauwe et. al. (1999), as well as the DOM-specific formulation proposed by Yamashita and Tanoue (2003). For the classic formulation,

$$DI = \sum_i \left[\frac{\mathrm{var}_i - AVG\ \mathrm{var}_i}{STD\ \mathrm{var}_i} \right] \times f\ accoef_i$$

where DI is the degradation index, var_i is the Mol%-AA_i, avg var_i and std var_i are the mean and standard deviation in their data set (Table 1, Dauwe et. al., 1999), and fac $coef_i$ is the factor coefficient for AA_i from the first axis in the same table.

For the DOM-specific formulation proposed by Yamashita and Tanoue (2003),

$$DI = \sum_i \mathrm{var}_i \times f\ accoef_i$$

where var_i is Mol%-AA_i and fac $coef_i$ is the factor coefficient of AA_i from the first axis (Table 4 and Figure 6, Yamashita and Tanoue, 2003). Variables for both formulations are shown below, in Table 1.

Table 1. **Variables for Two Degradation Index Formulations Compared in the Text**. Parameters used to calculate the Degradation Index using the DOM-specific formulation of Yamashita and Tanoue (2003) and the classic formulation of Dauwe et. al. (1999) are shown. The derivation and usage of each parameter are described above (section 2.6.3).

AA	Fac Coef *DOM*	Fac Coef *classic*	AVG	STD
ASP	-0.154	-0.102	13.4	2.7
GLU	0.146	0.065	10	2.3
SER	0.156	0.015	7.2	1.9
HIS	0.232			
GLY	-0.331	-0.099	17.6	3.8
THR	0.132	-0.129	7.1	1.5
ALA	-0.313	-0.043	11.8	0.8
VAL	0.358	-0.044	7.6	1.1
ILE	0.357	0.139	4.5	0.8
PHE	0.379	0.134	3.7	1.2
LEU	0.372	0.169	6.6	1.5

2.6.4. Statistical analysis

Statistical analysis was conducted using the JMP statistical software package (SAS, Version 12). Statistical significance of the difference between means was determined using t-tests, with significance levels stated in the text. Relationships between variables are described using orthogonal least-squares regressions, with the ratio of the x and y measurement error variance determined from univariate variance estimates of the x and y variables. Relevant p-values are noted in the text.

3. Results and Discussion

In recent years, the size class of detrital organic matter has been recognized as a main factor associated with both its reactivity and composition (e.g. Benner and Amon, 2015), and been shown to correlate directly with ^{14}C age distribution (Walker et al., 2011, Walker et. al. 2014, Walker et. al., 2016). The samples analyzed here for

amino acid enantiomers were isolated by sequential UF and SPE of the UF permeate (Broek et. al., 2016, Broek et. al., in prep.). The nitrogenous compounds in these samples therefore represent HMW vs. LMW fractions of the DON pool. The distribution of ^{14}C ages for these same samples clearly confirms this expectation (Supplementary Figure S1; Broek et. al., 2016, Broek et. al., in prep.). Specifically, the older ^{14}C ages and higher C:N elemental ratios for isolated LMW-DOM at all depths in the water column are consistent with both size-^{14}C age and size-reactivity ideas (Walker et al., 2016), as well as past observations (Benner and Amon, 2015, Walker et. al., 2011, Walker et. al., 2014).

This unique sample set therefore allows the first examination of DOM AA enantiomers in relation to directly measured ^{14}C ages. In the discussion that follows, we therefore discuss our results in the context of HMW isolates representing semi-labile DOM (SL-DOM), and LMW, SPE isolates as representing primarily R-DOM.

3.1. Amino Acid Enantiomers in Semi-Labile and Refractory DOM

Synthesis and incorporation of D-AAs are unique to prokaryotic organisms, providing a definitive tracer for microbial origin within the dominant DON compound class. There is a clear offset in average %D-enantiomer between SL-DOM and R-DOM for all AAs (Fig. 2). These average trends, with higher %D in SL-DOM for Ala and in R-DOM for all other AAs, are also present at individual sample depths (Table 2). As noted above, since there are clear ^{14}C age differences between all SL-DOM and R-DOM isolates, this progressive increase in %D across all D-AAs (except

Ala) with DOM age implies that the prokaryotic contribution increases with DOM age across the DOM size-reactivity continuum.

However, within this general pattern, we also identified a number of intriguing new patterns. First, we observed a broad decoupling of %D trends for Ala: while Ala had the highest %D-enantiomer of all chiral AAs in both size classes, its behavior with DOM age was the opposite that of all other D-AAs, having uniformly higher %D-Ala in SL-DOM (Fig. 2). This suggests not only that the dominant source of D-Ala is in the HMW (and relatively labile) DOM pool, but also that cycling of D-Ala is independent of the other D-AAs. If correct, this should also be supported by Mol% data, and also by direct correlations to ^{14}C age, and so we examine this hypothesis further below (see Sections 2 and 4).

In addition, beyond the four D-AAs that are commonly reported in DOM (Ala, Asp, Ser, and Glu), we also positively identified and quantified three additional D-AAs (Leu, Val, and Phe). While some prior work has suggested the presence of minor amounts of these compounds in HMW-DOM (McCarthy et. al., 1998), GC-FID data was not able to make definitive positive identifications: reported abundances were generally low and inconsistent, with these D-AAs either not identified, and/or indistinguishable from blanks. To our knowledge, no subsequent work has reported these D-AAs in DOM. In our data, GC-MS quantification with single ion monitoring unambiguously showed that these AAs were present in every sample, with low concentrations in HMW-DOM but strongly elevated concentrations in LMW-DOM (Fig. 2). These results, coupled with ^{14}C age relationships discussed below (Section 4)

suggest distinct sources and cycling behavior for these three "new" D-AAs with DOM age.

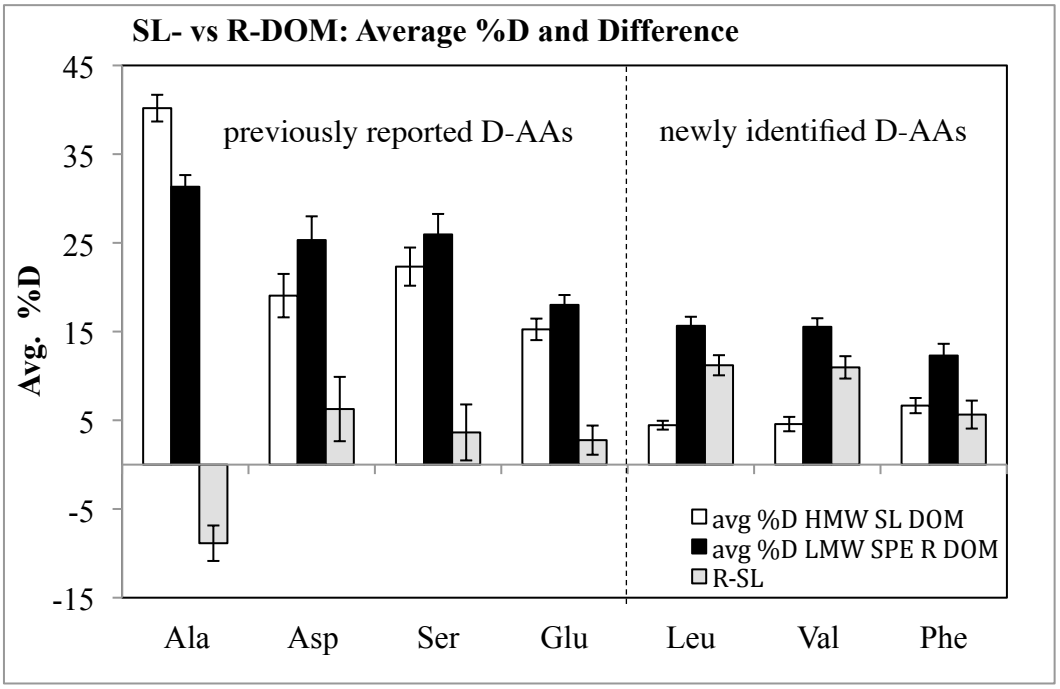

Figure 2. Average %D Amino Acids for Semi-Labile and Refractory DOM Fractions. The AA %D is higher in the refractory DOM fraction (LMW, older ^{14}C ages) vs. semi-labile DOM (HMW, younger ^{14}C ages) for all AAs except for Ala, which displays the opposite trend. "Previously reported" refers to D-AAs that have been commonly identified in the literature, in both HMW and total DOM. "Newly identified" refers to D-AAs confirmed in DOM here for the first time, based on GC-MS fragmentation patterns. White bars=%D in HMW-DOM, black bars=%D in LMW-SPE-DOM, gray bars=%D difference (LMW-HMW). Error bars represent the standard deviation of the mean across depth- and cruise-averaged %D for the size classes (N=8), and propagated error in the standard deviation of the mean for the difference. AA abbreviations are as defined in text.

Table 2. %D for Seven Amino Acids in HMW (Semi-Labile) and LMW (Refractory) DOM Fractions from Surface to Deep North Pacific Subtropical Gyre. A single analysis was performed for each depth, cruise, and DOM size fraction. Uncertainties are ±1 standard deviation in the propagated uncertainty of the racemization blank.

SPL	DEPTH	ALA	±	ASP	±	GLU	±	SER	±	LEU	±	VAL	±	PHE	±
SL-DOM	2	33.0	0.5	11	1	11.4	0.6	14.2	0.3	2.6	0.7	1	1	4	1
(HMW-UDOM)	400	41.0	0.5	16	1	14.2	0.6	18.8	0.3	3.6	0.7	6	1	5	1
summer	850	34.3	0.5	7	1	9.5	0.6	14.8	0.3	2.7	0.7	2	1	3	1
2014	2500	41.3	0.5	21	1	15.7	0.6	19.8	0.3	4.5	0.7	7	1	6	1
R-DOM	2	24.4	0.5	15	1	11.5	0.6	17.7	0.3	10.1	0.6	10	1	11	1
(LMW-SPE-DOM)	400	30.1	0.5	23	1	18.8	0.6	27.6	0.3	18.2	0.6	17	1	12	1
summer	850	31.3	0.5	21	1	18.7	0.6	30.8	0.3	14.3	0.6	15	1	6	1
2014	2500	30.7	0.5	18	1	18.1	0.6	18.3	0.3	16.3	0.6	17	1	10	1
SL-DOM	2	40.4	0.5	23	1	16.2	0.6	26.7	0.3	4.6	0.7	2	1	7	1
(HMW-UDOM)	400	44.0	0.5	24	1	17.7	0.6	28.0	0.3	5.6	0.6	6	1	9	1
spring	850	44.3	0.5	26	1	19.8	0.6	28.4	0.3	6.5	0.6	7	1	9	1
2015	2500	43.0	0.5	24	1	17.5	0.6	27.8	0.3	5.5	0.6	5	1	9	1
R-DOM	2	35.3	0.5	35	1	19.5	0.6	35.2	0.3	15.4	0.6	14	1	18.1	0.9
(LMW-SPE-DOM)	400	35.4	0.5	33	1	21.6	0.6	32.3	0.3	19.6	0.6	18	1	16.7	0.9
spring	850	29.0	0.5	24	1	15.6	0.6	22.6	0.3	14.5	0.6	15	1	11	1
2015	2500	34.4	0.5	33	1	20.4	0.6	23.2	0.3	16.8	0.6	19	1	13.2	0.9

The results for the four widely reported D-AAs (Ala, Asp, Ser, and Glu) confirm previous D-AA measurements in HMW-DOM (McCarthy et. al. 1998, Kaiser and Benner, 2008, Figure 3a). However, our direct measurements of the same D-AAs in LMW-DOM isolates are uniformly much lower than previously reported LMW-DOM values calculated by difference from whole water in the same ocean region (Fig. 3b; Kaiser and Benner, 2008). Several methodological differences could contribute to this contrast. First, the offset might be evidence of resin selectivity. While the PPL resin is not enantioselective, it is possible that D-AAs are disproportionately found in molecules that are poorly retained by the PPL resin, but are LMW, hydrolysable, and measurable in whole water. Bulk isotopic and elemental analyses generally indicate that LMW-SPE-DOM is representative of the larger LMW-DOM pool (Flerus et. al. 2012, Dittmar et. al. 2008), however bulk measurements would not necessarily reveal molecular-scale compositional differences. There is also some evidence for resin selectivity in bulk $\Delta^{14}C$ data, which shows that LMW-SPE-DOM is older than total LMW-DOM by ~300 years in the NPSG mesopelagic, and by close to ~1000 years at the surface (Broek et. al., in prep.). This suggests that some relatively fresh LMW material, along with high %D material, may not be retained by the resin. This non-retained material likely includes highly polar molecules (Flerus et. al., 2012), and also free AAs (Sipler and Bronk, 2015).

Alternatively, the difference between directly measured and calculated %D-Ala, Asp, Glu, and Ser results in LMW-DOM could reflect the character of the

material at the intersection of these compositionally different DOM pools. Our study used isolates at the higher end of commonly defined HMW-DOM (MW>2.5 kD), leaving all lower MW material to be extracted as LMW-SPE-DOM. Therefore, material with nominal MW from 1-2.5 kD is included as LMW-DOM in this study, but would be considered HMW-DOM in the prior results (Kaiser and Benner, 2008). This intermediate MW fraction is ~24% of total DOC throughout the water column in the Gulf of Mexico, and in the Mid-Atlantic Bight (Guo et. al., 1995). The higher %D in results calculated by difference therefore represents a lower MW fraction, which would be consistent with our results for all AAs excluding Ala across the size-reactivity continuum. Overall, our current data set cannot distinguish between methodological vs. environmental explanations for the difference between directly measured and calculated %D in LMW-DOM. The contrast in results suggests that additional experiments quantifying relative AA vs. D-AA yields using SPE resins would be required, combined with direct measurements of D-AAs in LMW-DOM. However, if SPE resins do in fact recover substantially less D-AAs in LMW-DOM, this observation in itself may provide new clues about the chemical identity of D-AA rich LMW molecules preserved in the deep ocean. We suggest that closer examination of chemical retention characteristics of SPE resins therefore might lead to new experiments designed to isolate this material.

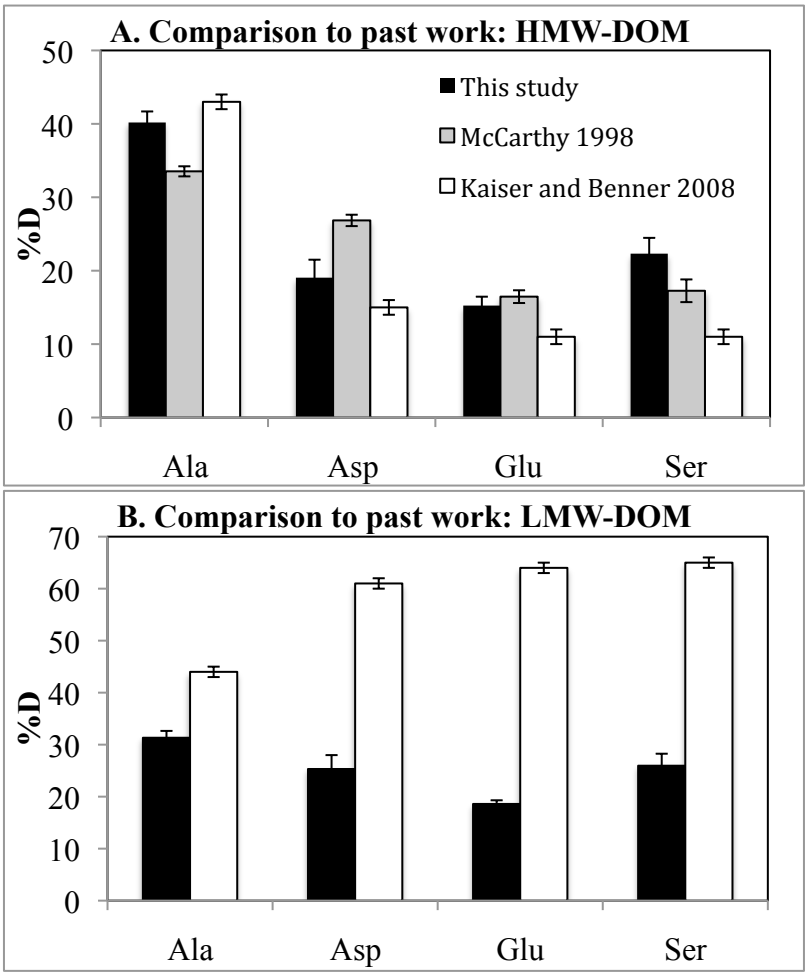

Figure 3. Average %D-AAs: Comparison with Past Work. Panel A (semi-labile; HMW-DOM). The %D results for four widely reported AAs (Ala, Asp, Glu, and Ser) in HMW-DOM agree with previous measurements in the NPSG. Black bars=this study, gray bars=McCarthy et. al., 1998, white bars= Kaiser and Benner, 2008. Panel B (refractory DOM; LMW-SPE-DOM): Measured %D for four widely reported AAs in LMW-DOM are lower than %D calculated by difference. Black bars=this study, white bars= Kaiser and Benner, 2008. Error bars represent standard deviation of the mean for data from this study (N=8) and McCarthy et. al., 1998 (N=4), or the range from depth integration for data from Kaiser and Benner, 2008. AA abbreviations are as defined in text.

In contrast with the four widely reported D-AAs, a much larger increase was observed for %D enantiomer of Leu, Val, and Phe between SL-DOM and R-DOM (Fig 2, Fig. 4). As noted above, early work tentatively identified these D-AAs in a number of HMW-DOM samples (McCarthy et. al., 1998). However, the relatively low abundance and inconsistent detection of these D-AAs made these identifications tenuous, and subsequent studies quantifying D-AAs in both HMW and total DOM have not reported these D-enantiomers. However, in this study, GC-MS with single ion monitoring allowed both positive identification as well as quantification of the D-Leu, D-Val, and D-Phe in every sample.

In HMW material, %D values were low (Fig. 4), at ranges generally comparable to %D values in those HMW-DOM samples for which these D-AAs were identified (McCarthy et. al., 1998). However, our direct measurements in LMW-DOM isolates indicate dramatically increased concentrations vs. HMW material (%D-Leu and –Val approximately triple, and %D-Phe values approximately double). Based on the ^{14}C ages of the size classes, these differences cannot be due to abiotic racemization alone. For example, abiotic racemization of Phe due to average age offsets between HMW and LMW-DOM would be expected to add ~1 %D to the initial value in HMW-DOM (Bada, 1971), while the difference between the size classes is approximately six fold greater. Though these D-AAs have previously received little attention, these dramatic increases in their enantiomeric ratios with increasing ^{14}C age (discussed in detail below; Section 4) suggest they may be extremely useful tracers for understanding microbial production of R-DOM.

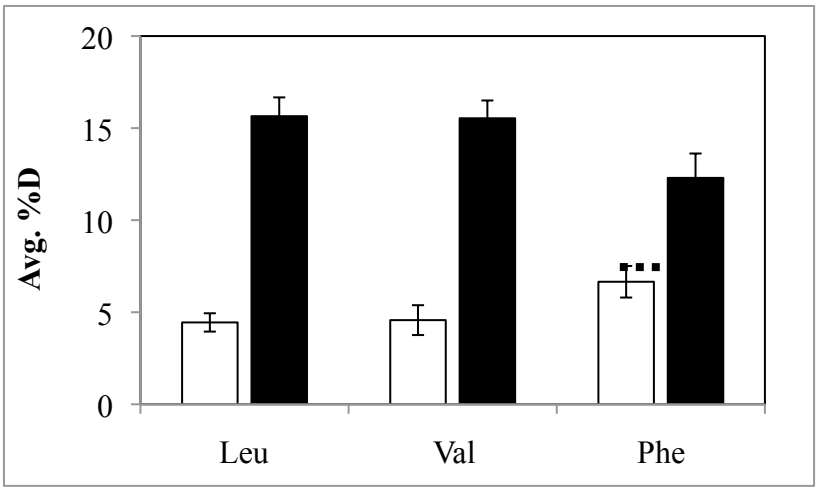

Figure 4. %D in Semi-Labile and Refractory DOM vs Abiotic Racemization. Three D-AAs that are rarely reported in HMW-DOM are strongly enriched in LMW-SPE-DOM. White bars=%D in HMW-DOM, black bars=%D in LMW-SPE-DOM. For Phe, the increase in %D due to abiotic racemization of HMW-DOM, calculated from the age difference between the size classes and the racemization kinetics for Phe in seawater (Bada 1971), is shown as a dashed line. Error bars represent standard deviation of the mean across depth- and cruise-averaged %D (N=8). AA abbreviations are as defined in the text.

3.2. Amino Acid Molar Percent Abundance Distributions

3.2.1. Alanine and Glycine Abundance: Unexpected Decoupling

Organic matter degradation is associated with systematic changes in AA-Mol% distributions. In particular, Mol%-Ala and -Gly are thought to increase with microbial degradation (Dauwe et. al. 1999, Lee et. al. 2000, Yamashita and Tanoue 2003, Calleja et. al. 2013). These two AAs show the greatest difference in Mol% between the isolated DOM size classes (Table 3; Fig. 5), but surprisingly, they have an inverse relationship. Mol%-Ala is ~10% lower in the LMW fraction, while Mol%-Gly is about ~6% higher. Although Mol%-Gly and -Ala are in fact positively

correlated with each other within LMW-DOM (R^2=0.57, p=0.03; Supplementary figure S-2A), the inverse relationship between isolated fractions suggests that Ala and Gly may in fact be associated with independent processes. Microbial "degradation" is a broad term that encompasses multiple independent processes, including addition of microbial biosynthate, selective removal, and molecular alteration (e.g. McCarthy et al., 2007). We therefore hypothesize that the opposite trends of Mol%-Ala and -Gly in our isolated fractions indicate that these AAs in fact trace different processes or microbial sources.

Table 3. Amino Acid Molar Percent Abundance Results. Uncertainties are ±10% of the Mol% value.

SPL	DEPTH	ALA	±	VAL	±	THR	±	GLY	±	ILE	±	SER	±	LEU	±	PRO	±	ASP	±	GLU	±	PHE	±
SL-DOM	2	23	2	3.2	0.3	6.8	0.7	14	1	2.5	0.2	13	1	5.0	0.5	3.6	0.4	15	2	8.4	0.8	2.5	0.2
(HMW-UDOM)	400	27	3	3.9	0.4	5.0	0.5	17	2	3.8	0.4	8.1	0.8	7.1	0.7	4.6	0.5	12	1	8.3	0.8	3.3	0.3
summer	850	23	2	4.6	0.5	5.0	0.5	17	2	4.2	0.4	4.3	0.4	6.7	0.7	5.2	0.5	16	2	10	1	3.2	0.3
2014	2500	39	4	3.0	0.3	4.8	0.5	18	2	2.0	0.2	5.2	0.5	3.2	0.3	3.1	0.3	14	1	5.6	0.6	2.0	0.2
R-DOM	2	12	1	5.3	0.5	5.7	0.6	20	2	4.2	0.4	8.9	0.9	6.5	0.7	7.6	0.8	15	1	11	1	4.4	0.4
(LMW-SPE-DOM)	400	15	2	5.6	0.6	3.7	0.4	28	3	4.0	0.4	7.6	0.8	5.5	0.5	6.3	0.6	14	1	7.7	0.8	2.3	0.2
summer	850	17	2	6.3	0.6	4.0	0.4	32	3	4.3	0.4	3.7	0.4	7.2	0.7	10	1	6.4	0.6	6.9	0.7	2.8	0.3
2014	2500	13	1	5.2	0.5	3.4	0.3	26	3	3.7	0.4	3.0	0.3	6.1	0.6	6.8	0.7	15	1	15	1	3.1	0.3
SL-DOM	2	18	2	2.3	0.2	5.8	0.6	20	2	1.9	0.2	11	1	5.5	0.5	4.3	0.4	17	2	10	1	3.5	0.3
(HMW-UDOM)	400	29	3	2.3	0.2	3.7	0.4	27	3	1.6	0.2	8.0	0.8	3.2	0.3	3.7	0.4	14	1	6.6	0.7	1.7	0.2
spring	850	24	2	2.4	0.2	4.3	0.4	26	3	1.6	0.2	7.6	0.8	3.0	0.3	4.4	0.4	17	2	8.4	0.8	1.7	0.2
2015	2500	14	1	2.0	0.2	3.9	0.4	23	2	1.8	0.2	7.4	0.7	4.7	0.5	5.2	0.5	22	2	13	1	3.3	0.3
R-DOM	2	14	1	4.1	0.4	3.4	0.3	23	2	2.9	0.3	7.6	0.8	6.7	0.7	7.9	0.8	15	2	10	1	4.8	0.5
(LMW-SPE-DOM)	400	15	1	3.6	0.4	4.2	0.4	30	3	2.2	0.2	6.9	0.7	4.0	0.4	6.0	0.6	17	2	10	1	1.8	0.2
spring	850	14	1	5.5	0.5	4.1	0.4	24	2	3.4	0.3	7.6	0.8	6.6	0.7	7.4	0.7	15	1	9.3	0.9	3.4	0.3
2015	2500	12	1	4.4	0.4	2.4	0.2	27	3	2.8	0.3	14	1	5.5	0.5	6.2	0.6	15	2	8.7	0.9	2.3	0.2

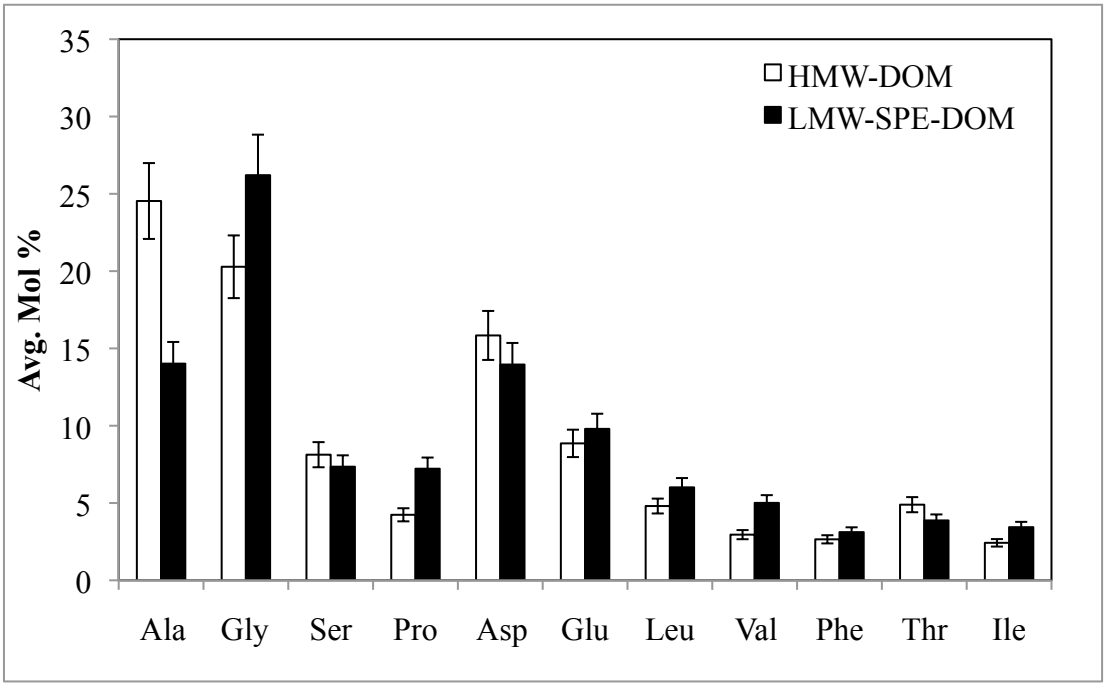

Figure 5. Comparison of Amino Acid Molar Percent Abundance in Semi-Labile vs. Refractory DOM Fractions. White bars represent HMW-DOM (SL-DOM), black bars represent LMW-DOM (R-DOM). Contributions of most AAs are similar for both fractions, however Mol%-Ala decreases while Mol%-Gly increases with age. Mol%-Pro,-Leu, -Val, and –Ile increase slightly; changes are significant at the 1% level for Ala, Gly, Val, and Pro; at the 2% level for Ile; and at the 5% level for Leu. Each bar represents depth and cruise averaged Mol% values, and error bars represent the average error for analysis (± 10% of the Mol% value). AA abbreviations are as defined in the text.

For Ala, the coupled decrease in both Mol% and %D from HMW- to LMW-DOM together suggest that there is a source of Ala to HMW-DOM, strongly enriched in the D-enantiomer, which is not effectively transferred to the LMW-SPE-DOM pool during degradation. Perhaps the most likely microbial source biomolecule satisfying these conditions is peptidoglycan, a structural polymer of D- and L-AAs and amino sugars that is a major component of bacterial cell walls (Schliefer and Kandler, 1972, McCarthy et al., 1998). This HMW polymer has been also shown to be semi-labile in seawater, with particularly rapid remineralization of the peptide component after hydrolysis (Nagata et. al., 2003). While previous work has suggested that intact peptidoglycan subunits constitute <0.1% of DON (Kaiser and Benner, 2008) there are several reasons why this material could be a more significant fraction of HMW-DON as measured in our current study. First, concentration of peptidoglycan in the HMW-DOM fraction, as indicated by Mol% and %D trends between the DOM size classes, would be expected to increase its analytical signal relative to its contribution to total DOM, since only 10-25% of DOM is HMW (Benner et. al. 1997, Walker et. al., 2011, Benner and Amon, 2015). In particular, for samples used here, the explicit goal was to use very high UF concentration factors, in order to isolate the youngest, highest MW-DOM for a SL-DOM endmember (~10% of total DOC; Walker et. al., 2011).

Additionally, the previous low estimates for peptidoglycan contribution to DON likely reflects only intact peptidoglycan, because it relies on ratios of molecularly identifiable muramic acid (Mur) as well as D-AAs (Kaiser and Benner,

2008). However, degradation studies of radiolabeled peptidoglycan have indicated that Mur is rapidly modified during peptidoglycan degradation, such that most degraded sugar moities can no longer be identified by standard chromatographic techniques (Nagata et. al., 2003). Together, these studies suggest that most peptidoglycan in the dissolved phase would likely be both partially degraded and structurally modified, with most fragments moving outside traditional analytical windows. Our coupled results for Mol% and D-Ala therefore seem consistent with peptidoglycan as a major bacterial N source primarily to SL-DOM, decreasing rapidly with degradation into the LMW, R-DOM pool. However, we note that if most degraded peptidoglycan fragments are in fact rapidly modified, it would be difficult to derive meaningful quantitative estimates of peptidoglycan contributions from molecular tracers alone.

Finally, although Ala is the most abundant AA in peptidoglycan, Gly is abundant in this polymer as well (Schliefer and Kandler, 1972). While Gly has no chirality, the opposite trends in Mol% of these AAs suggest different cycling mechanisms. If our observations of Mol% and %D trends for Ala confirm the results of controlled degradation experiments showing that the peptide component of peptidoglycan is quickly remineralized (Nagata et. al., 2003), then the higher Mol% Gly in older, LMW-DOM fraction may indicate more diverse sources for Gly. Alternately, preferential removal of other AAs vs. Gly could drive the higher Mol%-Gly in older DOM. This would likely be accompanied by other indications of heterotrophic activity, such as increases in compounds such as D-Asp and D-Ser, so

far identified as occurring only in heterotrophic bacteria (Kaiser and Benner, 2008). However, the general similarity of %D values for these particular AAs in our HMW vs. LMW material does not strongly support this latter hypothesis. Overall, at this stage we can only conclude that Mol% trends between HMW and LMW-DOM for Ala and Gly suggest that these AAs trace different aspects of microbial degradation, with Ala dominance in HMW-DOM likely indicating fresh bacterial inputs, and Gly accumulation in LMW-DOM acting as a more general indicator of more diverse microbial source or degradation. We note that this general conclusion is also consistent with relationships between Mol% and $\Delta^{14}C$ for these same AAs, which show Mol%-Ala decreasing with age (R^2=0.46, p=0.006, Supplementary Table 1), but Mol%-Gly increasing with age (R^2=0.38, p=0.01, Supplementary Table 1). However, future compound-specific $\Delta^{14}C$ measurements will be needed to truly test size-age relationships for these AAs.

3.2.2. Other Amino Acids: Molar Percent Abundance Trends with Bioavailability

In addition to the large Mol% changes for Ala and Gly, there are also smaller but significant changes in Mol% of Leu, Val, Pro, Phe, and Ile between the size classes (p=0.01 for Val and Pro, p=0.02 for Ile, and p=0.05 for Leu). The Mol% values of these AAs are also all positively correlated with each other, across the entire sample set (slopes for regressions of all pairings range: 0.50-1.98, R^2 values range: 0.10-0.82; Supplementary Figure S-2 B-E). The similar trends in abundance across this group of AA parallel previously reported relationships along a coastal to ocean

upper-water column transect in bulk DOM (Yamashita and Tanoue, 2003). These former results were interpreted as driven by general degradation, and Leu, Val, Phe, and Ile were interpreted as representing relatively more bioavailable AAs in bulk DOM. However, our data based on central Pacific depth profiles shows these same AAs having higher Mol% in older, more refractory LMW-DOM, and lower Mol% in the younger, HMW-DOM.

The higher Mol% of Leu, Val, Phe, and Ile in older, LMW-DOM would seem to directly contradict the prior interpretation based on transect data, and could have several explanations. First, it is possible that shifting biological sources, from coastal eukaryotic to open ocean prokaryotic primary producers, are at least partially responsible for Mol% changes in Leu, Val, Phe, and Ile observed along the ocean transect represent and attributed to degradation (McCarthy et. al. 2004). Recent work has also demonstrated that different phytoplankton strains produce suites of DOM with very distinct distributions of size, polarity, and structural features, suggesting likely differences in AA profiles based on variation in plankton community structure as well (Becker et. al., 2014). Therefore, differences in DOM autotrophic sources characteristic of contrasting ocean biomes could lead to significant inaccuracies in interpretation of changes assumed to result from degradation alone.

3.2.3. Degradation Index Correlations

The degradation index (DI) is a multivariate approach to using synoptic changes in multiple AA Mol% to indicate relative degradation state of marine organic matter (Dauwe, et al., 1999). DI has become one of the most widely used organic

matter degradation proxies in sediments and particles (e.g., McCarthy et al., 2007, Batista et al., 2014), and an alternate version has also been proposed for DOM (Yamashita and Tanoue, 2003). If DI in fact functions in DOM to indicate increasing degradation, and if Mol% offsets we observed between HMW and LMW-DOM are linked to increasing heterotrophic bacterial alteration, we would expect DI to have substantial and consistent offsets between isolated SL- and R-DOM fractions. We examined this prediction using two versions of DI: the original DI formulation, based on an operational comparison of particles and different sediments along an assumed continuum of degradation (Duawe, et al., 1999), and an alternate version with coefficients determined specifically for DOM by Yamashita and Tanoue (2003), based on the coastal to the open ocean transect noted above.

3.2.3a. Relationship with Total %D-AAs

The range of DI values for both size-reactivity classes (Figure 6, Supplementary Figure 3) generally agree with previously published ranges for both the classic (Dauwe et. al., 1999, Davis and Benner, 2005, Calleja et. al., 2013) and DOM-specific (Yamashita and Tanoue, 2003) DI formulations. There are a few exceptions to this, most notably in several HMW-DOM samples with DI below the previously published ranges, which in principle would indicate more extensive degradation in SL-DOM vs. total DOM. However, it is most likely that this results from the fact that Ala, with its strongly negative DI coefficient, is concentrated in the HMW-DOM samples. There is a negative correlation between DI values and total %D across the entire sample set, consistent with greater bacterial contribution to more

degraded DOM. The correlation is stronger in the formulation developed by Yamashita and Tanoue (R^2=0.67, p=0.0001; Figure 6a) than in the original DI formulation of Dauwe et. al. (1999) (Supplementary Figure 3a, R^2=0.54, p=0.001). These results are consistent in linking both operational DI indices with increasing prokaryotic D-AAs, within the size-reactivity framework.

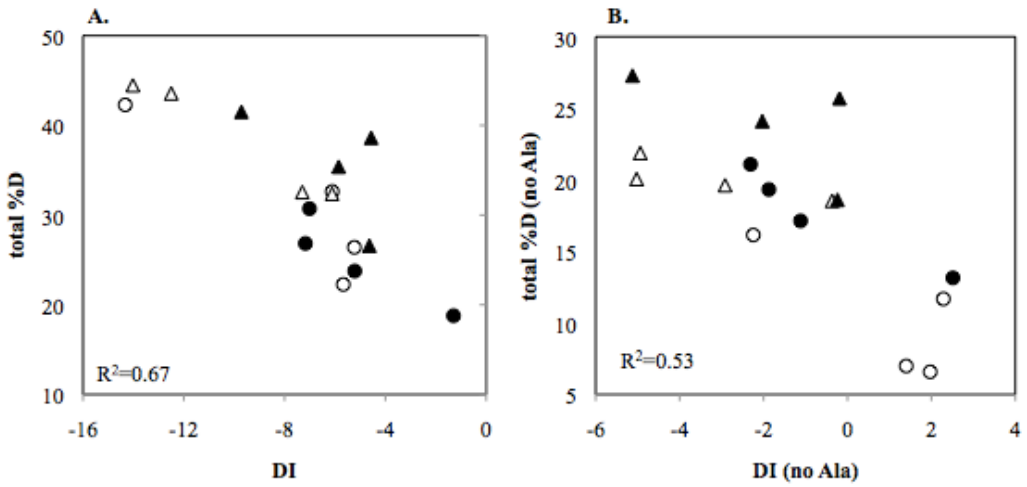

Figure 6. **Relationships Between Degradation Index (DI) and total %D Amino Acids**. Panel A: Total %D-AAs correlate strongly (p<0.0001) with degradation indicated by DI, with higher %D in more degraded samples. DI indicates HMW-DOM is the more degraded DOM fraction. Panel B: Strong offsets between the DOM fractions in mol% Ala and %D Ala hide otherwise similar relationships between DI and total %D-AAs (excluding Ala) (p=0.001). DI values were calculated using the formulation of Yamashita and Tanoue (2003). Total %D-AAs are calculated from measured %D of each amino acid, weighted by its Mol%. Open symbols= HMW-DOM, closed symbols=LMW-SPE-DOM, circles=summer 2014, triangles=spring 2015.

However, an unexpected aspect of this relationship between DI and total %D across the DOM fractions is that HMW-DOM in general has more negative DI values and higher total %D, nominally placing the younger, HMW-DOM fraction on the

more “degraded” end of the spectrum. The concentration of Ala (and D-Ala) in HMW-DOM drives this surprising offset. The high concentration and %D of Ala in HMW-DOM affects not only the total %D value, but the DI value as well through the negative DI coefficient of Ala (Table 1). When Ala is excluded from the calculation of both DI and total %D, there is no separation between HMW- and LMW-DOM DI values, while the significant negative correlation is maintained (Figure 6b, R^2=0.53; p=0.001). This result using the DOM-specific DI formulation is again similar to the analogous relationship using the classic Dauwe et al. (1999) formulation, but in this case, the result using original classic DI formulation is substantially weaker (Supplementary Figure S-3b, R^2=0.16, p=0.13). These observations are consistent with our hypothesis above (Section 2.1), that semi-labile sources of Ala, having high %D-Ala (such as peptidoglycan) are concentrated in the HMW-DOM fraction, and not effectively transferred to LMW-DOM. Finally, the similar slopes for the relationship between DI and %D across both HMW and LMW-DOM when Ala is excluded (Figure 6b) strongly suggest a universal relationship between synoptic AA Mol% and %D changes, reinforcing the conclusion that Ala is unique, with distinct sources and cycling in marine DOM.

Overall, these results suggest that the formulation of DI developed specifically for DOM from transect data by Yamashita and Tanoue (2003) traces the accumulation of prokaryotic AAs in DOM. Without Ala, there is a strong and significant relationship between decreasing DI and increasing %D for all other D-AAs in DOM. However, at the same time, the lack of any clear differentiation within

the %D vs. DI plots based on size-age class is puzzling. It suggests that current DI formulations are not strongly tied to DOM ages, and so calls into question the linkage of DI to commonly understood ideas of "degradation" in the global DOM pool.

3.2.3b. Relationship with $\Delta^{14}C$

In fact, DI is not significantly correlated with $\Delta^{14}C$ age of DOM (R^2=0.01, p=0.65 using the formulation of Yamashita and Tanoue; R^2=0.14, p=0.15 using the formulation of Dauwe et. al.; see Supplementary Figures S-3c and S-4a). Excluding Ala from the DI calculation only decreases the correlation (R^2=0.06, p=0.36 using the formulation of Yamashita and Tanoue, or R^2=0.03, p=0.49 using the formulation of Dauwe et. al.; see Supplementary Figures S-3d and S-4b). These results indicate that "degradation," as tracked by the Mol% changes synthesized by DI indices, is actually mostly independent of DOM age. This is puzzling, given the clear correlation between %D and DI (excluding Ala).

We hypothesize that the poor correlation between DI and $\Delta^{14}C$, despite the correlation with total %D, is most likely due to variation in the relationships between %D, Mol%, and $\Delta^{14}C$ for individual AAs (see Supplementary Table 1, and Section 3.4 below). Together, the DI, $\Delta^{14}C$, and %D results further suggest that while the specific AA abundance changes reflected in existing DI formulations clearly indicate prokaryotic input, they do a poor job of reflecting "degradation", or the progressive formation of R-DOM material on long ocean timescales.

3.2.4. DI_{14C}: A New Degradation Index for Refractory DOM Formation

Aiming to understand the disconnect in the relationship %D, Mol%, and $\Delta^{14}C$, an analysis of the relationships between Mol% and $\Delta^{14}C$ for each of the seven chiral AAs individually (see Supplementary Table 1) shows that Mol% Ala and Ser are positively correlated with $\Delta^{14}C$ (R^2=0.46 for Ala, R^2=0.68 for Ser, $p<0.01$ for both), while Mol%-Val is negatively correlated with $\Delta^{14}C$ (R^2=0.41 p=0.08), and Leu, Asp, Glu, and Phe are not correlated with $\Delta^{14}C$ ($p\geq0.4$). The Mol% Gly, a known indicator of microbial degradation, is also negatively correlated with $\Delta^{14}C$ (R^2=0.38, p=0.01, see section 2.1). When coefficients are added to unify the slopes of the relationship between Mol% and $\Delta^{14}C$ for Gly, Ala, Val, and Ser, and the sum of the resulting adjusted Mol% values are plotted against $\Delta^{14}C$, this new DI, DI_{14C}, accounts for 91% of the variance in the data set (Figure 7). Two outlier points were removed for this analysis, one with anomalously high Mol% Ala (>3 standard deviations above the mean Mol% Ala for this data set), and one with anomalously high Mol% Ser (>2 standard deviations above the mean Mol% Ser for this data set).

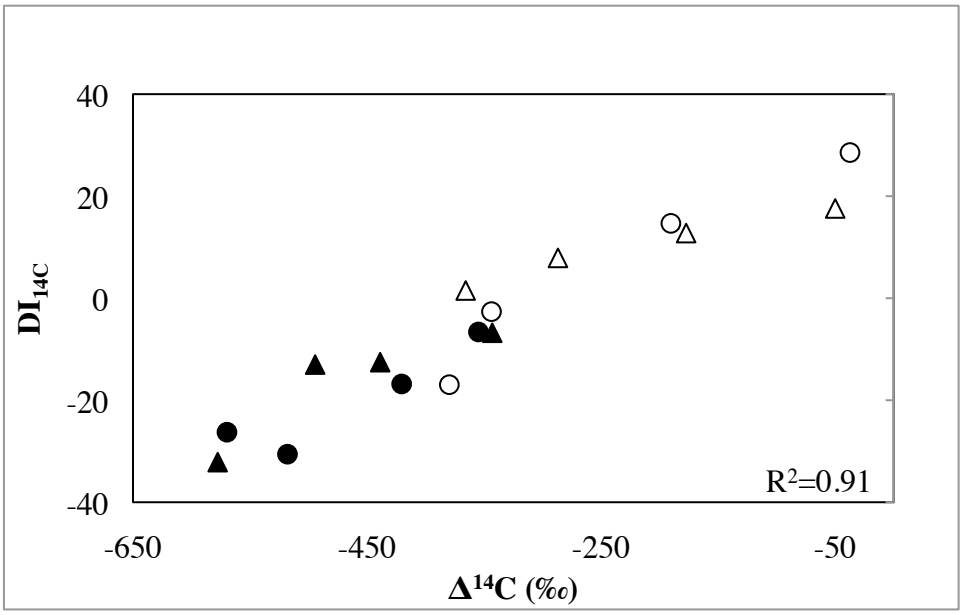

Figure 7: DI_{14C} Has a Strong Relationship with Bulk $\Delta^{14}C$. The new DI is Mol%Ala-Mol%Gly+2.5Mol%Ser-4Mol%Val. Open symbols= HMW-DOM, closed symbols=LMW-SPE-DOM, circles=summer 2014, triangles=spring 2015.

Overall, despite the simplicity of the derivation of these coefficients, the resulting correlation with $\Delta^{14}C$ (R^2=0.91, $p<0.001$) suggests a tremendous improvement over previous DI formulations, in terms of indicating R-DOM formation. Of course, just as in development of the original DI indices, in this new formulation a good correlation with $\Delta^{14}C$ is expected, since AAs were chosen based on the strength of those relationships. The major difference is that in prior DI formulations, coefficients were derived based on an operational and somewhat descriptive sample ordering, from assumed "fresh" to assumed "degraded". In contrast here, our sample ordering is based on measured $\Delta^{14}C$ ages. While future work will be required to test the robustness of our new parameters based on the DOM

size-reactivity fractions, we hypothesize that is should better reflect the relative lability of the specific bacterial compounds introduced into oceanic DOM.

Together, this exercise suggests that $\Delta^{14}C$ and total %D are indicators for fundamentally different aspects of degradation, a conclusion that is strongly supported by comparisons of the relative coefficients for individual AA within different DI formulations. The most notable difference in DI coefficients is for Ala, which has a negative coefficient in conventional DI formulations (indicating more extensive degradation), but a positive coefficient based on the relationship between Mol% and $\Delta^{14}C$ across the DOM fractions. As discussed above, Ala appears to trace bacterial inputs that are largely labile (See section 2.1). For Ser, the positive coefficient in DI_{14C} is consistent with past DI formulations, indicating greater abundance in less degraded material, while the negative correlation for mol% Val with DI_{14C} is in agreement with the formulation or Dauwe et. al. (1999), but not with that of Yamashita and Tanoue (2003). Interestingly, Phe and Leu are among the AAs with the largest magnitude positive coefficients (indicating enrichment in fresher material) in both previous DI formulations, however, these are not correlated with $\Delta^{14}C$. Overall, we suggest that these relationships may lead a more mechanistically grounded view of compositionally distinct prokaryotic sources to the SL- and R-DOM in relation to DOM degradation and age.

3.3. %D and Mol%: Linked Indicators of Bacterial Source?

A somewhat unexpected aspect to our data set is a strong linkage between %D and Mol% across the entire size/age spectrum of marine DOM (Figure 8 a, b). At the individual AA level, AAs with low Mol% have lower %D, regardless of season, depth, or size class. Overall, the relationship between %D and Mol% is remarkably consistent, including identical slopes for HMW and LMW-DOM, while the intercepts are offset by ~8% D. Because of the greater number of D-AAs we have measured here, including the newly confirmed D-AAs that exist at low concentrations in both size classes (Sections 1 and 2 above), this relationship likely could not have been identified in past work. At the same time, the fact that all AAs measured fit closely into the same relationship provides further evidence for the accuracy the new D-AAs (Phe, Val and Leu) quantified here.

The remarkably unified relationship across all AAs strongly links bacterial source and concentration for the seven chiral AAs quantified in this analysis. This in turn suggests that across the size/age spectrum of DOM, the most abundant AAs are disproportionately from non-protein bacterial sources. Relationships between AAs on this spectrum also suggest relative quantitative importance of individual AAs for prokaryotic-source DON.

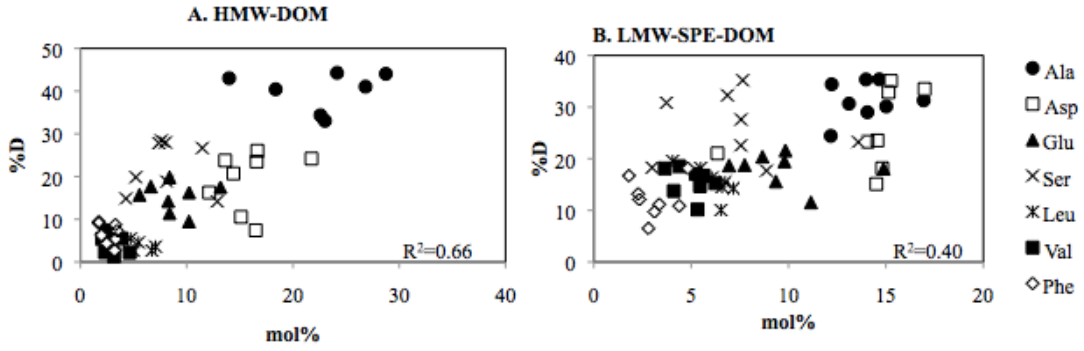

Figure 8: Strong Positive Correlation Between Molar Percent Abundance and %D Across All Amino Acids in Both DOM Size Classes. Each point represents a single sample. AA abbreviations are as defined in the text. Panel A, slope=1.7±0.3 %D mol%$^{-1}$, intercept=0±1 %D. Panel B, slope=1.8±0.6 %D mol%$^{-1}$, intercept=6±2 %D.

3.4. D-Enantiomer Variation with DOM $\Delta^{14}C$

This data set allows us to directly test of the microbial N pump hypothesis for the first time using trends in the abundance of bacterial biomarkers across a range of DOM ages, both within and across the isolated DOM size classes. We hypothesize that a continuous relationship between %D and $\Delta^{14}C$ would indicate progressively increasing in microbial AA sources down the size-reactivity continuum, with slopes reflecting relative rates of input for individual D-AA sources. In contrast, size-based discontinuities might indicate distinct sources or other processes within HMW vs. LMW DOM pools.

Across all samples, there are significant regressions ($p \leq 0.1$) between D-enantiomer abundance and $\Delta^{14}C$ with non-zero slopes for all AAs except Asp and Ser (Figures 9, 10). For all AAs except Ala, slopes are negative (Figure 10), indicating a progressive increase in %D with decreasing DOM $\Delta^{14}C$, consistent with microbial N pump ideas. In contrast, Ala alone appears to have the opposite relationship with

$\Delta^{14}C$ (Figure 9). The offsets between the mean %D values for HMW- and LMW-DOM are also significant for all AAs, at the 1% level for Ala, Leu, Val, and Phe; at the 10% level for Asp and Glu; and at the 15% level for Ser.

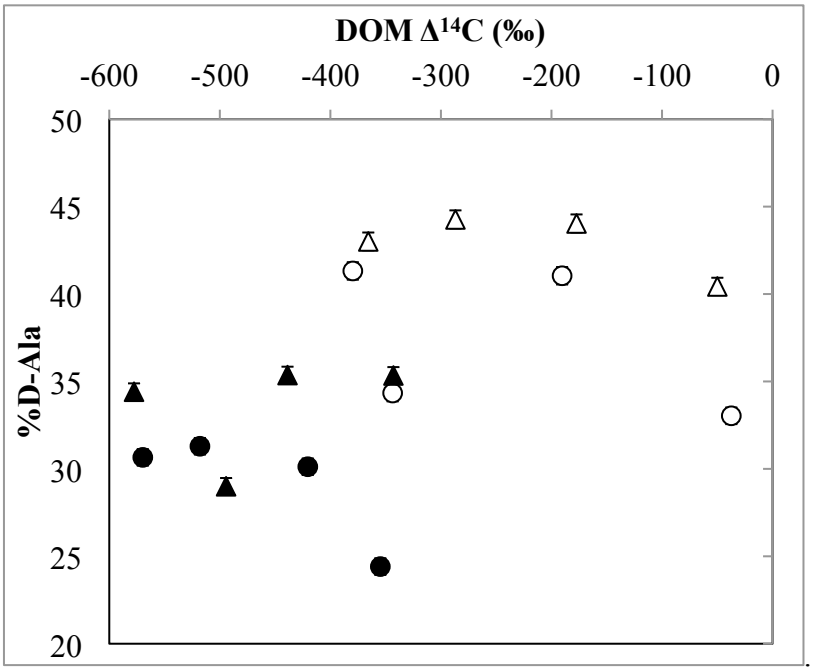

Figure 9. Percent D-Alanine Change with DOM $\Delta^{14}C$. %D-Ala decreases with DOM $\Delta^{14}C$ between the size classes (R^2=0.21 including all samples, or 0.62 when surface samples are excluded). Each point represents a single sample. Open symbols= HMW-DOM, closed symbols=LMW-SPE-DOM, circles=summer 2014, triangles=spring 2015. Error bars show the propagated uncertainty in the racemization blank (±1 SD).

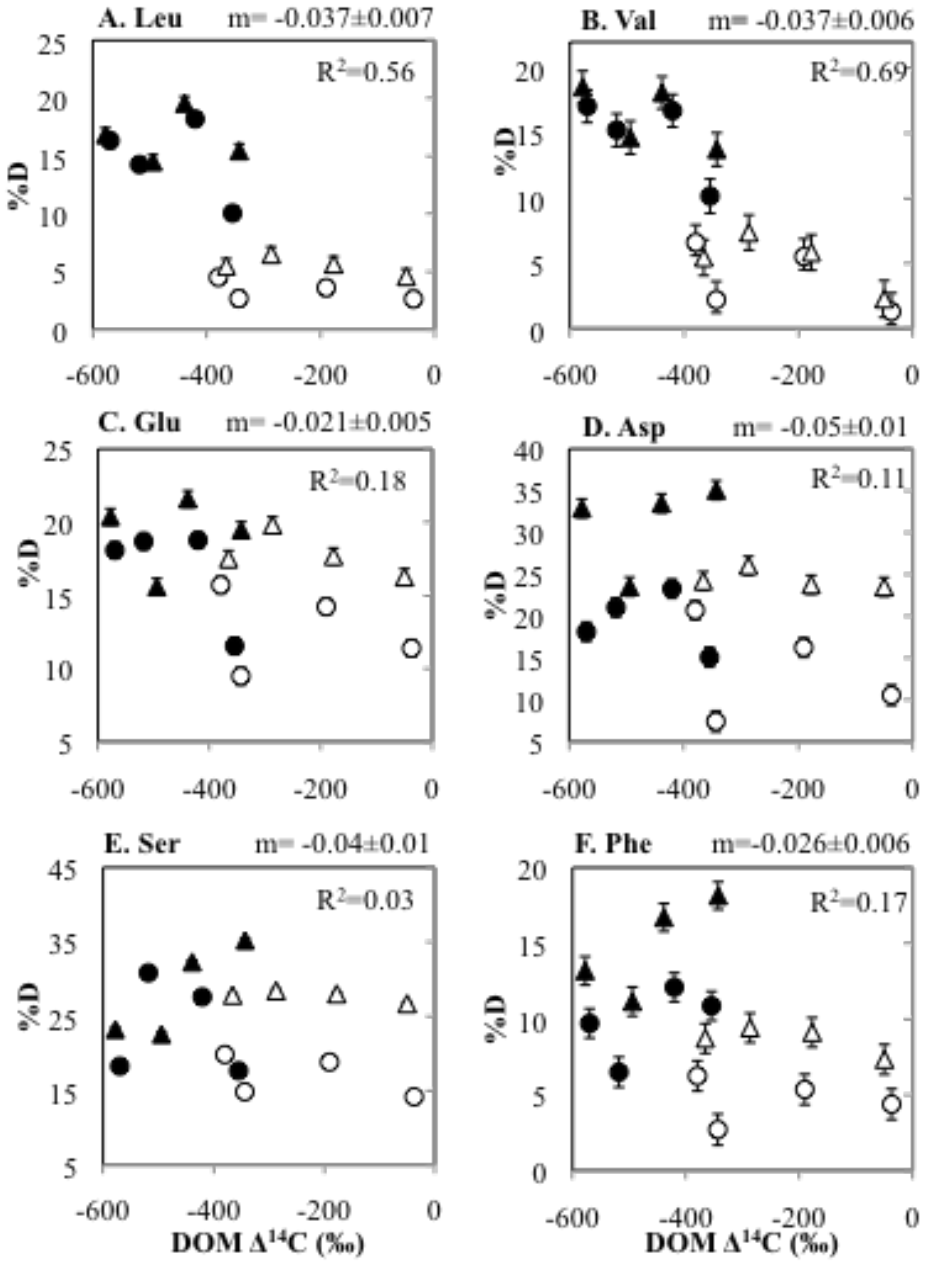

Figure 10. Percent D Enantiomer Change with DOM $\Delta^{14}C$ for All Amino Acids Apart from Alanine. %D generally increases with age for all other AAs, however strength of correlation varies between AAs. Each point represents a single sample. Open symbols= HMW-DOM, closed symbols=LMW-SPE-DOM, circles=summer 2014, triangles=spring 2015. "m" is the slope in the regression, in %D $‰^{-1}$. Error bars show the propagated uncertainty in the racemization blank (±1 SD). AA abbreviations are as defined in the text.

The relationship between %D-Ala and $\Delta^{14}C$ has a significant positive slope (R^2 =0.21, p= 0.08), indicating elevated %D-Ala values in progressively younger material, with decreasing %D-Ala in older material (Figure 9). While the strength of the relationship across all data is modest, it becomes substantially stronger when surface samples are excluded (R^2=0.62; p=0.002). This result seems consistent with our hypothesis that D-Ala concentrations are highly dependent on the input of an Ala-rich source (such as peptidoglycan) to HMW-DOM, which undergoes fairly rapid degradation. It is interesting to note, however, that the main structure in the $\Delta^{14}C$ versus %D-Ala data (Figure 9) suggests an offset between the two DOM size-reactivity fractions, as opposed to a smooth continuum. This in turn supports the idea that HMW, semi-labile, D-Ala-rich compounds are rapidly degraded (or modified) in the upper water, such that %D-Ala does not display a continuous progression with $\Delta^{14}C$.

In contrast to D-Ala, all other D-AAs increase in %D with more negative $\Delta^{14}C$, suggesting progressive accumulation of D-AAs with ^{14}C age. However, the variation in slopes of the %D and $\Delta^{14}C$ relationship for different AAs also suggests important differences in cycling dynamics, which maybe related to different molecular sources for individual D-AAs (Figure 10). For example, slopes for D-Leu (-0.037±0.007 %D ‰$^{-1}$) and D-Val (-0.037±0.006 %D ‰$^{-1}$) are indistinguishable, and are far better constrained than all other D-AAs (slope<0 with p≤0.001 for Leu and Val, or p≥0.1 for other AAs). This suggests that D-Leu and D-Val may trace similar bacterial biomolecules. It further suggests that, on the global ocean time scale

represented by surface to deep water comparison in the North Pacific Subtropical Gyre, the microbial contributions tracked by Leu and Val increase rapidly with depth. Val is also the only AA for which correlations between %D and $\Delta^{14}C$ are significant within the size classes as well (p=0.07 for LMW-DOM, or 0.14 for HMW-DOM). Taken together, these observations suggest D-AA subgroupings may represent unique tracers for major bacterial D-AA biomolecular sources.

3.5. D-AA Water Column Structure

Contrasting relationships between $\Delta^{14}C$ and %D for different AAs suggest there could also be differences between D-AA depth profiles. While consistent depth structure in %D has typically not been reported for the four previous widely observed AAs (Ala, Asp, Glu, and Ser) in either HMW or total DOM (McCarthy et. al. 1998, Dittmar et. al. 2001, Nagata et. al. 2003, Pérez et. al. 2003, Kaiser and Benner 2008, Kaiser and Benner 2009), our observations of distinct age vs. %D relationships could suggest variable D-AA depth structure, which would most likely only be observable for those D-AAs having the steepest slopes in %D vs. $\Delta^{14}C$ relationships (Fig. 9). Put another way, on the scale of large $\Delta^{14}C$ changes across our sample set, only D-AAs showing relatively rapid change on timescales of water column mixing would be likely have oceanographically consistent depth structure.

In fact, clear depth structure in the central Pacific water column was observed only for D-Leu and D-Val, closely matching these expectations (Fig. 11; Supplementary Figure S-5). In the HMW fraction, there is no clear depth structure for D-Leu. However, the %D-for both Leu and Val in LMW-DOM increase strongly

from the surface to 400 m, then decrease to near-surface values at 850 m, and increasing again slightly from 850 to 2500 m. These trends for both AAs were replicated in profiles from two independent cruises, in two differing oceanographic periods. For D-Val, the HMW-DOM depth trend appears essentially identical, apart from the single 850 m value from the summer cruise. However, given that seasonality would not be expected to strongly influence DOM composition at this depth, we are unsure if significant weight should be given to this single value.

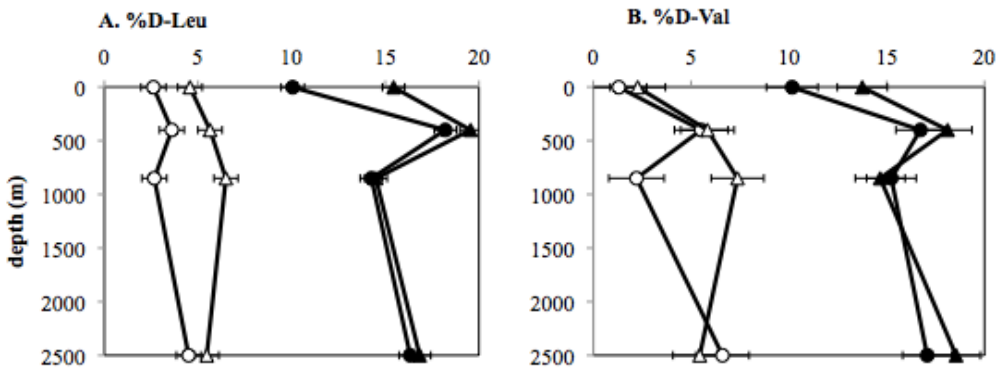

Figure 11. Depth Structure in Enantiomeric Composition of Leucine and Valine in HMW- vs. LMW-DOM Fractions. The depth structures of %D-Leu (Panel A) and %D-Val (Panel B) are shown. Each point represents a single sample. Open symbols= HMW-DOM, closed symbols=LMW-SPE-DOM, circles=summer 2014, triangles=spring 2015. Error bars show the propagated uncertainty in the racemization blank (±1 SD). AA abbreviations are as defined in the text.

Overall, these results are remarkably consistent with relative slopes observed in $\Delta^{14}C$ vs. %D regressions (Figure 10). Further, the apparent similarity in cycling of these two AAs is also consistent with correlations between their Mol% values discussed above (see Section 2). The peaks of %D at 400m occurs in the "twilight zone", the region of maximum particle flux attenuation, where sinking material from

the euphotic zone is most rapidly remineralized by heterotrophic bacteria (Buesseler et. al., 2007). While we do not have detailed profiles to assess if this 400m in fact represents the exact "peak", rapid increases in %D for Leu and Val from surface to 400m likely represents input of fresh, particle-derived heterotrophic bacterial DOM.

In contrast to D-Leu and D-Val, as noted above no other D-AAs show clear depth structure in either MW fraction (Supplementary Figure S-5). Similar to prior published results, no depth structure was observed for the four higher concentration D-AAs (Ala, Glu, Ser, Asp) previously reported in HMW and total DOM (McCarthy et. al. 1998, Nagata et. al. 2003, Pérez et. al. 2003, Kaiser and Benner 2008, Kaiser and Benner, 2009). Similarly, no depth structures as observed for other D-AAs in LMW-DOM, potentially because of the low %D changes with $\Delta^{14}C$, possibly indicating that freshly produced LMW-DOM has similar %D to the more refractory LMW-DOM already present. Phe, the other AA designated as especially bioavailable by DI indices, also consistently decreases in %D from 400 to 850 m in LMW-SPE-DOM, but the increase from in %D from surface to 400 m is not consistently present for Phe. Phe is different from Leu and Val based on the relationship between %D and $\Delta^{14}C$, as well.

4. Conclusions

To test the "microbial N pump" hypothesis, we measured AA enantiomers and Mol% distributions, and evaluated these data in conjunction with ^{14}C ages of independently isolated semi-labile (HMW) and refractory (LMW) DOM fractions. Because D-AAs are unambiguous biomarkers for prokaryotic sources in the largest

identifiable compound class of DON, this unique sample set allowed the first direct assessment of the variation in prokaryotic contributions to DON across the size-reactivity continuum, from the surface to deep ocean in the North Pacific Subtropical Gyre. Our results strongly support the idea that prokaryotic organisms represent a major source of R-DOM, and that bacteria progressively change DOM on timescales of ocean-wide circulation.

At the same time, our D-AA data also revealed a number of surprising results. First, while we observed the four D-AAs widely reported previously in marine DOM (Ala, Asp, Glu, and Ser) in all samples, GC-MS analysis of large-volume isolates also allowed us to quantify four additional D-AAs (D-Leu, D-Val, and D-Phe) in both HMW and LMW-DOM at all depths. Despite the lower concentrations of these newly confirmed D-AAs, their %D depth profiles are consistent with their $\Delta^{14}C$ and Mol% patterns, confirming that these are real compounds, with unique tracer potential. Our results therefore expand the suite of common D-AAs in marine DOM from four to seven. Most importantly, we also observed consistent, but unique relationships between %D, Mol%, and $\Delta^{14}C$ among different D-AAs, suggesting that a number of key D-AA subgroupings may represent unique proxies for specific bacterial sources.

D-Ala emerged as a unique AA within many aspects of the data set. Consistent with previous reports, D-Ala was the single most abundant D-AA. However, in contrast to the trends in %D with $\Delta^{14}C$ for all other D-AAs, we observed lower %D-Ala in R-DOM. This distinct relationship was accompanied by analgous

Mol% trends, with lower Mol% Ala (but higher mol% Gly) in LMW-DOM. We therefore hypothesize that D-Ala cycling is strongly linked to semi-labile peptidoglycan material, which is relatively rapidly degraded in surface waters, as opposed to the more diverse bacterial origins, and slower degradation rates, for the other D-AAs.

In contrast to D-Ala, all other AAs increased in %D with ^{14}C age. However, the increase in %D from SL- to R-DOM was most significant for the three newly-confirmed D-AAs (Phe, Leu, Val), suggesting these may in fact be the best D-AA tracers for bacterial contribution to the DON pool. Further, D-Val and D-Leu were the only two D-AAs with clear water column structure, consistent with their $\Delta^{14}C$ relationships, which indicate relatively rapid changes in %D for these AAs. Maxima in the upper mesopelagic strongly suggest a direct linkage to sinking particle sources. We therefore hypothesize that D-Val and D-Leu might be developed as new tracers for bacterially mediated linkage between PON and DON pools in the mesopelagic and deep ocean.

This data set also allowed comparison of degradation in DOM as assessed by $\Delta^{14}C$, total %D, and Mol%-based degradation indices, potentially offering new insights into the mechanistic underpinnings of these different degradation indicators. While total %D and conventional DI indexes are negatively correlated, the variable relationships between $\Delta^{14}C$, Mol%, and %D for individual AAs cause prior DI indices to conflict with $\Delta^{14}C$ results, and be inconsistent with the wider DOM size-age continuum. We therefore used relationships between AA-Mol% and $\Delta^{14}C$ to

develop DI_{14C}, which we show more accurately reflects DOM $\Delta^{14}C$ in our DOM size-reactivity fractions. Further, the surprisingly strong correlation between Mol% and %D when all quantified chiral AAs are considered together links D-enantiomer abundance with increasing molar concentration across the DON age-size spectrum. This observation suggests that combining the Mol%/$\Delta^{14}C$ correlations used to develop DI_{14C} , together with relationships between these variables and %D, could allow a novel mechanistic understanding of increasing contributions of bacterial biomolecules to the DOM pool over time, in contrast to prior DI indices, which were based on operational comparisons of samples along an assumed, but poorly quantified, continuum of "degradation".

Taken together, our data set strongly supports the microbial N pump hypothesis, and at the same time demonstrates a very significant expansion in the tracer potential for D-AAs in ocean DOM. The progressive increases in D-enantiomers with ^{14}C age, spanning approximately 6000 years of ^{14}C age, indicate that formation for R-DON is not only intimately linked with bacterial sources, but also that the process of bacterial modification operates continuously on timescales of ocean mixing. We suggest that future work aimed at understanding specific molecular sources of different D-AAs found in ocean DOM could lead to a far more detailed mechanistic view of the processes that form R-DON in the oceans.

Most broadly, our results again emphasize the critical role that prokaryotic organisms play in ocean biogeochemical cycles, and particularly in formation of R-DON. Because a changing DOM reservoir size would directly affect atmospheric

CO_2, the microbially mediated N sequestration indicated by our data also suggests a positive feedback for climate change: expanding microbially-dominated ecosystems could exacerbate N-limitation, further limiting primary production and C sequestration. We suggest that future work focused on understanding the magnitude of this effect, as well as exploring detailed compositional differences along the DOM size-age continuum. Specifically, direct measurement of size-age relationships for AAs with contrasting trends in %D are needed to determine the scale at which bulk DOM cycling paradigms cease to apply.

Supplementary Figures and Text

Figure S-1. Size-Age Relationships

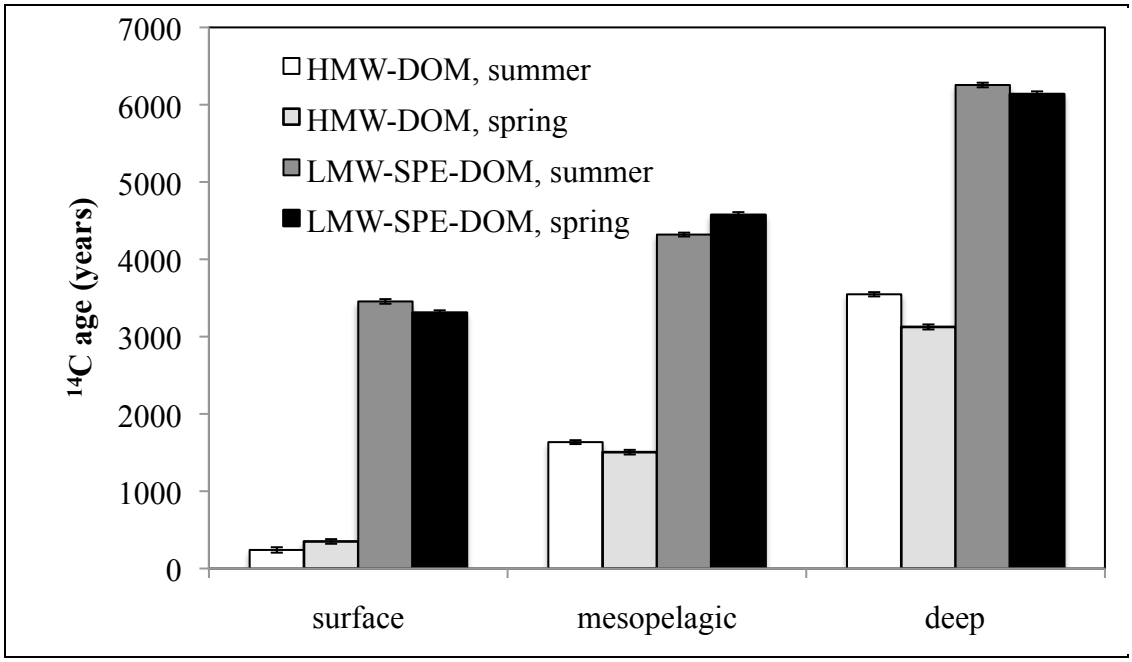

Figure S-1. Comparison of ^{14}C ages for DOM size classes. Data adapted from Broek et al., in prep.). Light bars represent HMW DOM, darker shaded bars represent LMW-DOM, collected from four independent cruises, from surface, mesopelagic (400m) and deep ocean. "Deep" bars here represent the average ages of samples from both 850 and 2500m. Error bars show AMS instrumental uncertainty of ±1 SD. LMW-SPE-DOM is older than HMW-DOM at all depths, supporting the designation of LMW-SPE-DOM as refractory DOM (R-DOM), and HMW-DOM as semi-labile DOM (SL-DOM). The HMW-DOM ranged from 240-3775 years old from surface to deep Pacific, while the LMW-SPE-DOM ranged from 3310-6860 years old at the same depths. Overall, both size classes were observed to increase in age from surface to depth, with a nearly constant age offset of ~3000 years throughout the water column, consistent with the size-reactivity continuum (e.g., Benner and Amon, 2015), and size-age continuum (Walker et al., 2016) ideas. Mass balance analyses using bulk radiocarbon and stable C and N isotopes also showed that the HMW- and LMW-SPE-DOM isolates together are representative of total DOM (Broek et. al., in prep).

Figure S-2. Molar Percent Abundance Correlations

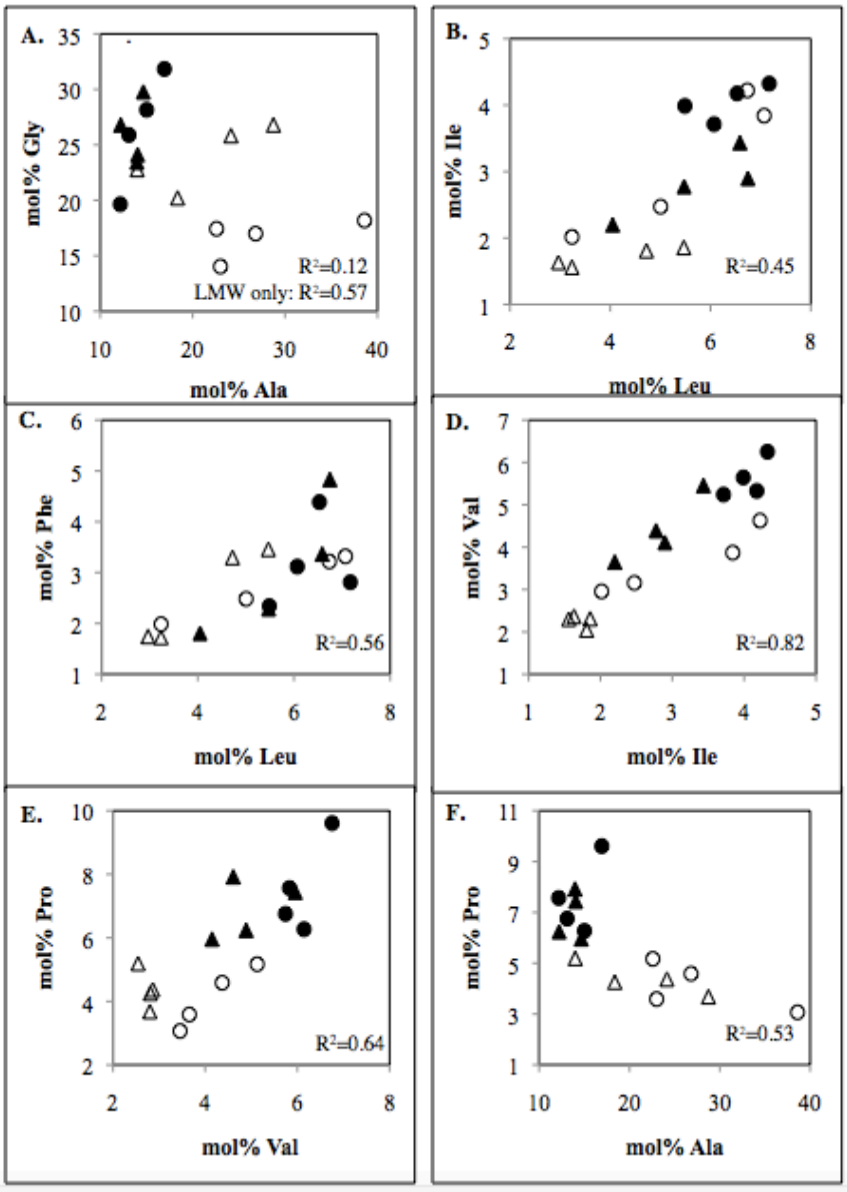

Figure S-2. Mol% Correlations. Mol% Val, Leu, Ile, Phe, and Pro are positively correlated (p=0.004 for Leu/Ile; p=0.003 for Leu/Phe; p=0.0001 for Ile/Val; p=0.0002 for Val/Pro). These AAs are thought to be especially bioavailable in DOM (Yamashita and Tanoue, 2003), although they have higher Mol% in LMW-SPE-DOM then in HMW-DOM. They are negatively correlated with Mol%-Ala (p=0.002 for Pro), but there are no consistent correlations between the Mol% of these AAs and Mol% Gly. Mol%-Ala and Gly are negatively correlated between size classes (p=0.1), but positively correlated within LMW-SPE-DOM (p=0.03). High Mol%-Ala and Gly are thought to be indicative of microbial degradation. Open symbols= HMW-DOM, closed symbols=LMW-SPE-DOM, circles=summer 2014, triangles=spring 2015.

Figure S-3. Degradation Index (DI) Correlations with Total %D-AAs and Bulk $\Delta^{14}C$ Using the Classic DI Formulation of Dauwe et. al. (1999)

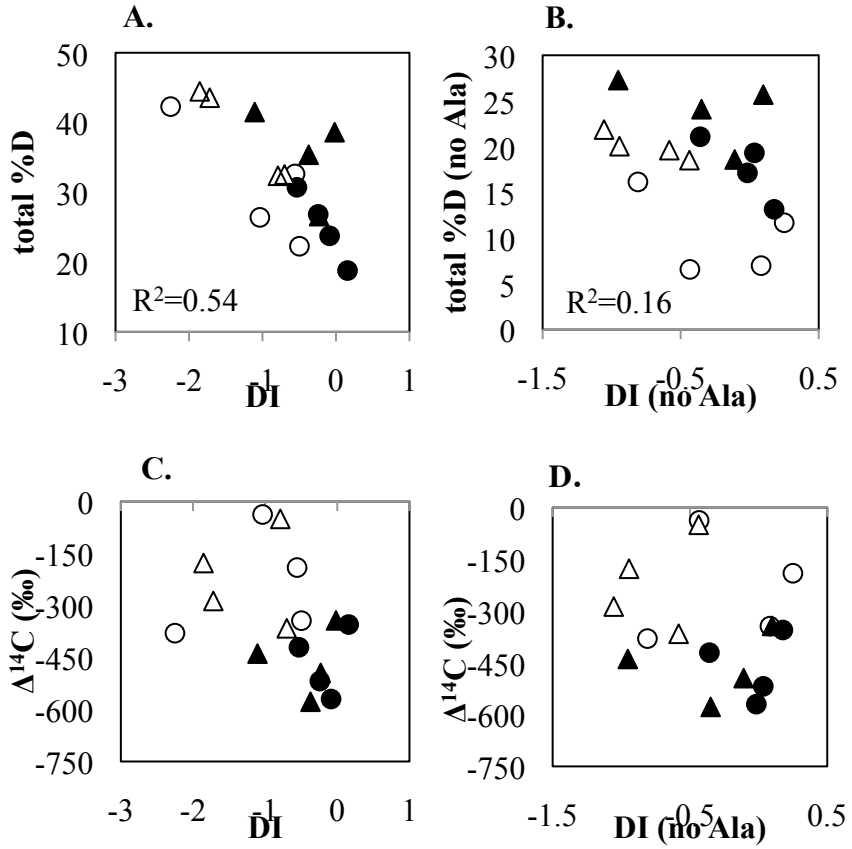

Figure S-3. The DI using the classic formulation developed by Dauwe et. al. (1999) yields similar correlations with total %D-AAs and bulk $\Delta^{14}C$ as the DOM-specific DI formulation of Yamashita and Tanoue (2003). Panel A. Total %D-AAs increases with degradation based on DI, but HMW-DOM appears more degraded. Using the DI formulations developed by Dauwe et. al. (shown here) and Yamashita and Tanoue (Figure 6a) respectively, R^2=0.54 and 0.67; p=0.001 and 0.0001. Panel B. When Ala is excluded from both DI and total %D-AA calculations, the relationship between DI and total %D-AAs is similar in both size classes. Using the DI formulations developed by Dauwe et. al. (shown here) and Yamashita and Tanoue (Figure 6b) respectively, R^2=0.16 and 0.54; p=0.13 and 0.001. Panel C. DI and bulk $\Delta^{14}C$ are not correlated in either DI formulation. Using the DI formulations developed by Dauwe et. al. (shown here) and Yamashita and Tanoue (supplementary figure S-4a) respectively, R^2=0.14 and 0.01; p=0.15 and 0.65. Panel D. When Ala is excluded, there no relationship between DI (excluding Ala) and bulk $\Delta^{14}C$. Using the DI formulations developed by Dauwe et. al. (shown here) and Yamashita and Tanoue supplementary figure S-4b) respectively, R^2=0.03 and 0.06; p=0.49 and 0.36. Open symbols= HMW-DOM, closed symbols=LMW-SPE-DOM, circles=summer 2014, triangles=spring 2015.

Figure S-4. Little Relationship Between DI and $\Delta^{14}C$ Using the DOM-Specific DI Formulation of Yamashita and Tanoue (2003)

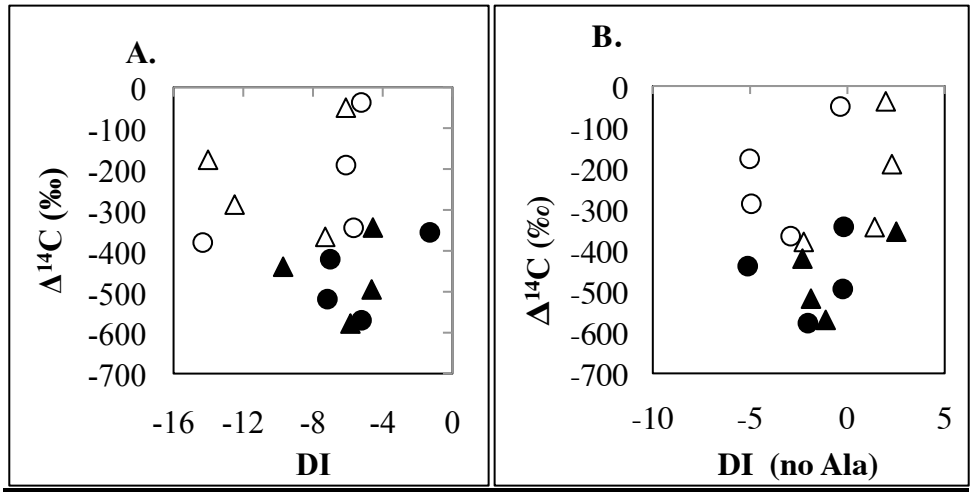

Figure S-4. Relationships between Degradation index (DI) and bulk $\Delta^{14}C$ using the DOM-specific DI formulation of Yamashita and Tanoue (2003) are weak. Panel A: DI and bulk $\Delta^{14}C$ are not correlated. R^2= 0.01 and p= 0. Panel B: When Ala is excluded, the correlation is still weak. R^2=0.06 and p=0.36. Open symbols= HMW-DOM, closed symbols=LMW-SPE-DOM, circles=summer 2014, triangles=spring 2015.

Figure S-5. No Depth Trends for D-AAs Other Than Leucine and Valine

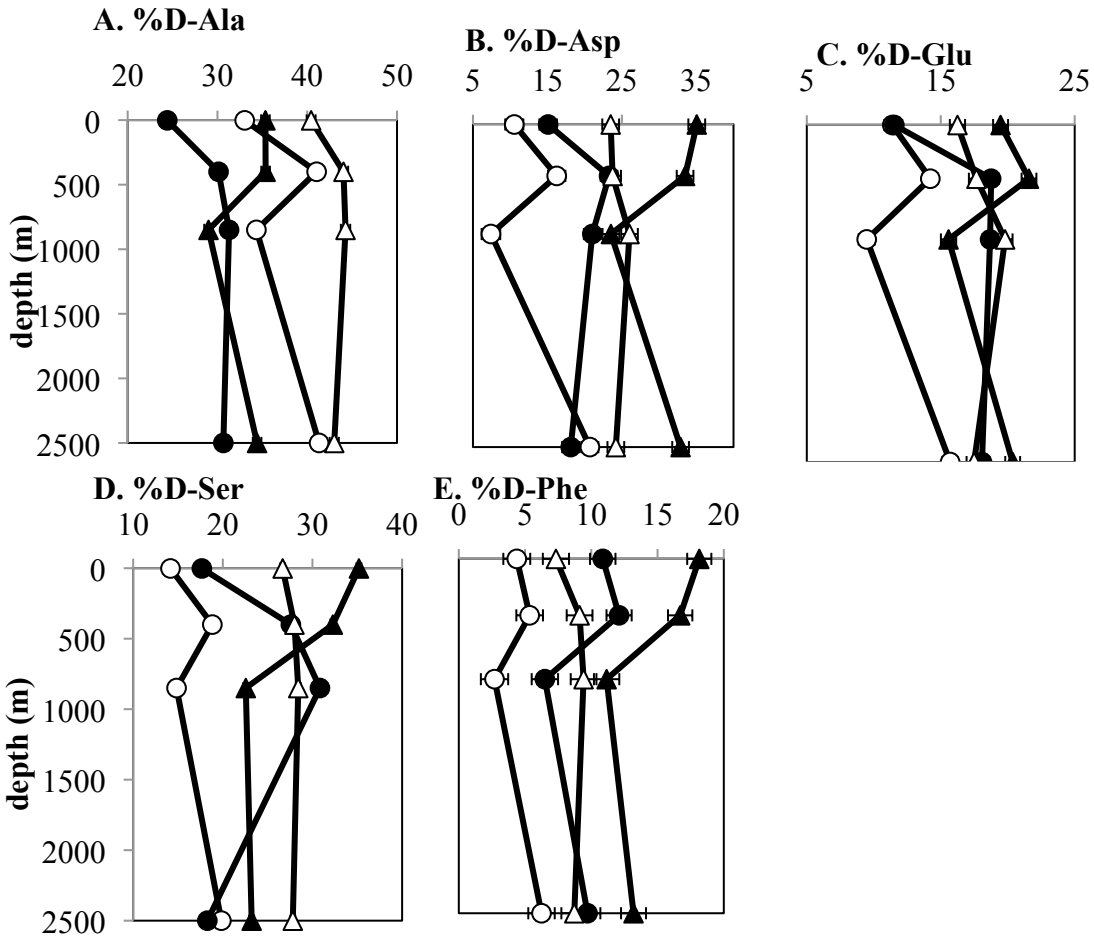

Figure S-5. No clear depth structure in percent D-enantiomer is present in HMW- or LMW-DOM for AAs with slow changes in %D with $\Delta^{14}C$ as compared to Leu and Val. Each point represents a single sample. Open symbols= HMW-DOM, closed symbols=LMW-SPE-DOM, circles=summer 2014, triangles=spring 2015. Error bars show the propagated uncertainty in the racemization blank (±1 SD). AA abbreviations are as defined in the text.

Table S-1. Regression information.

AA	Mol% vs $\Delta^{14}C$			%D vs Mol%		
	m (Mol%/‰)	R^2	p	m (%D/Mol%)	R^2	p
Ala	0.03	0.46	0.006	1.074	0.33	0.03
Asp	0.02	0.03	0.5	2.49	0.02	0.6
Glu	-0.01	0.05	0.4	-1.47	0.00	0.9
Ser	0.02	0.68	0.0002	-2.50	0.00	0.8
Leu	-0.01	0.05	0.4	4.35	0.05	0.4
Val	-0.01	0.41	0.008	4.52	0.4	0.009
Phe	0.01	0.00	1	4.60	0.02	0.6
Gly	-0.03	0.38	0.01	-	-	-
Pro	-0.01	0.42	0.006	-	-	-
Ile	-0.01	0.17	0.1	-	-	-

Table S-1. Regression information for individual AA Mol%, %D, and DOM $\Delta^{14}C$ relationships. Relationships that are significant at the 5% level are highlighted. $\Delta^{14}C$ vs %D relationships are shown in Figures 9-10.

Appendix 1: Detailed Racemization Correction

The measured %D is corrected for racemization during hydrolysis and derivatization according to Kaiser and Benner (2005).

(i) Determination of sample racemization during hydrolysis.

The %D racemization caused by liquid-phase hydrolysis at 110°C for 20 hr is shown in Table 1 of Kaiser and Benner (2005). We use the average value listed for each AA, which represents the average of the highest and lowest racemization observed in proteins (BSA and lysozyme) and free AAs. The standard deviation associated with this value is the population standard deviation of the values used in the calculation of the average:

(Eq. 1) $$\sigma_p = \sqrt{\frac{\sum (x - \bar{x})^2}{n}}$$

where σ_p is the population standard deviation in hydrolysis-induced racemization (%D), x is the hydrolysis-induced racemization for the free AA or the protein with the greatest racemization, $\bar{x}$ is the mean of the two values, and n is the number of samples in the population used to calculate the average (2). This gives the following values for hydrolysis-induced racemization:

AA	%D	σ
ALA	1.2	0.55
VAL	1.4	1.4
SER	0.3	0.3
LEU	1.6	0.65
ASP	4.4	1.2
GLU	2	0.6
PHE	1.7	0.95

(ii) Determination of sample racemization during derivatization.

The racemization caused by derivatization, including one esterification at 110°C for 60 min and two trifluoroacetylations at 100°C for 15 min each, were determined using free L-AA mixed standards, which were added to the sample preparation stream at the derivatization step. Injections of ~3 pmol/μL provided the optimal balance of separation and detectable D-AA peaks. Calibration standards may also be used to determine the derivatization racemization, if they have undergone both trifluoroacetylations. The racemization derivatization is the average %D in these derivatized standards, and the standard deviation in this value is the sample standard deviation of the derivatization racemization in these standards:

(Eq 2) $$\sigma_s = \sqrt{\frac{\sum (x - \bar{x})^2}{n-1}}$$

where σ_s is the sample standard deviation in derivatization-induced racemization (%D), x is the derivatization-induced racemization for a single standard, $\bar{x}$ is the mean derivatization-induced racemization for all standards for which this is measurable, and n is the number of standards used to calculate the average (at least 3). Derivatization racemization for samples prepared in different batches is typically equivalent within ±1σ; a set of reference values from one sample set is shown below.

AA	%D	σ
ALA	0.29	0.05
VAL	0.09	0.02
SER	0.6	0.1
LEU	0.5	0.1
ASP	0.39	0.09
GLU	0.3	0.2
PHE	0.3	0.3

(iii) Total sample preparation racemization.

The total sample preparation racemization (%D) is the sum of the hydrolysis and derivatization racemization. The uncertainties are propagated using standard procedures:

(Eq 3) $$\sigma_T = \sqrt{\sigma_H^2 + \sigma_R^2}$$

where σ_T is the standard deviation in the total sample preparation racemization (%D), and σ_H and σ_R are the standard deviations in the hydrolysis and derivatization-induced racemization, respectively.

(iv) Racemization-corrected %D.

The racemization-corrected %D is calculated using equation 7 of Kaiser and Benner (2005):

(Eq 4) $$L_0 = \frac{L_m - D_m\left(\frac{D}{L}\right)_b}{1 - \left(\frac{D}{L}\right)_b}$$

where L_0 is the racemization-corrected pmol L-AA injected, L_m and D_m are the measured (uncorrected) pmol L- and D-AA injected, and $\left(\frac{D}{L}\right)_b$ is the D/L ratio of the total sample preparation blank. The %D value of the total racemization blank is converted to D/L form according to

(Eq 5) $$\left(\frac{D}{L}\right)_b = \frac{\%D_b}{100 - \%D_b}$$

where $\%D_b$ is the total racemization blank in %D form. The racemization-corrected pmol D-AA injected is then calculated as

(Eq 6) $$D_0 = L_m + D_m - L_0.$$

The racemization-corrected %D is then

(Eq 7) $$\%D = 100 \times \left(\frac{D_0}{D_0 + L_0}\right) = 100 \times \left(\frac{D_0}{D_m + L_m}\right).$$

The standard deviation in this value is calculated by propagating the error in the racemization blank $\left(\frac{D}{L}\right)_b$ through equation 4. The standard deviation in L_0, the racemization-corrected pmol L-AA injected, is

(Eq 8) $$\sigma_{L_0} = \left(\frac{L_m - D_m\left(\frac{D}{L}\right)_b}{1 - \left(\frac{D}{L}\right)_b}\right)\sqrt{\left(\frac{\sigma_b}{1 - \left(\frac{D}{L}\right)_b}\right)^2 + \left(\frac{D_m\sigma_b}{L_m - D_m\left(\frac{D}{L}\right)_b}\right)^2}$$

where σ_b is the standard deviation in $\left(\frac{D}{L}\right)_b$. The standard deviation in the racemization-corrected pmol injected for each L-AA, σ_{L_0}, is also the standard deviation in the racemization-corrected pmol injected for the corresponding D-AA.

The racemization-corrected %D is calculated according to equation 7, and the standard deviation associated with the racemization-corrected %D is then

$$\textbf{(Eq 9)} \qquad \sigma_{\%D} = \frac{100}{L_m + D_m}\sigma_{L_0}.$$

Appendix 2. Amino Acid Enantiomers in Marine Particles

I also measured the %D-AAs in 16 POM filter samples collected by H. Close. The only AA with %D consistently greater than zero was Ala, which seems to have higher %D at deeper depths and in smaller size fractions. AAs other than Ala have measurable D-AA peaks, but they go away with the racemization correction and associated uncertainty. The %D-Ala values for two sample sets are shown below.

batch	depth (m)	cutoff (µm)	filter, notes	%D-Ala	SD
1	150	0.7	GF/F	0.6	0.6
1	150	0.2	Supor	2.2	0.6
1	150+155	1	QMA - sed trap	0.8	0.6
1	390	0.2	Supor	2.6	0.6
1	850	0.7	GF/F - pre-UF	1.9	0.6
1	850	0.2	Supor - pre-UF	1.6	0.6
1	1200	0.7	GF/F	2.5	0.6
2	25	0.7	GF/F	0.3	0.6
2	25	0.2	Supor	1.4	0.6
2	150	0.7	GF/F	0.5	0.6
2	150	0.3	GF75	0.8	0.6
2	150	0.2	Supor	2.3	0.6
2	400	0.7	GF/F	1.9	0.6
2	400	0.2	Supor	2.7	0.6
2	1195	0.7	GF/F	2.6	0.6
2	1195	0.3	GF75	3.7	0.5

References

Aluwihare, L.I., Repeta, D.J., Pantoja, S., Johnson, C.G., 2005. Two chemically distinct pools of organic nitrogen accumulate in the ocean. Science 308, 1007-1010.

Arrieta, J.M., Mayol, E., Hansman, R.L., Herndl, G.J., Dittmar, T., Duarte, C.M., 2015. Dilution limits dissolved organic carbon utilization in the deep ocean. Science 348, 331-333.

Bada, J.L., 1971. Kinetics of the nonbiological decomposition and racemization of amino acids in natural waters, in: Hem, J.D. (Ed.), Nonequilibrium Systems in Natural Water Chemistry. American Chemical Society, Washington, D.C., pp 309-331.

Batista, F.C., Ravelo, A.C., Crusius, J., Casso, M.A., McCarthy, M.D., 2014. Compound specific amino acid $\delta^{15}N$ in marine sediments: A new approach for studies of the marine nitrogen cycle. Geochim. Cosmochim. Acta 142, 553-569.

Becker J.W., Berube P.M., Follett C.L., Waterbury J.B., Chisholm S.W., DeLong E.F., Repeta D.J., 2014. Closely related phytoplankton species produce similar suites of dissolved organic matter. Front. Microbiol. 5, DOI=10.3389/fmicb.2014.00111.

Benner, R., Biddanda, B., Black, B., McCarthy, M., 1997. Abundance, size distribution, and stable carbon and nitrogen isotopic compositions of marine organic matter isolated by tangential-flow ultrafiltration. Mar. Chem. 57, 243-263.

Benner, R., Ziegler, S., 1999. Do photochemical transformations of dissolved organic matter produce biorefractory as well as bioreactive substrates?, in: Bell, C.R., Brylinsky, M., Johnson-Green, P. (Eds.), Microbial Biosystems: New Frontiers. Proceedings of the 8th International Symposium on Microbial Ecology. Atlantic Canada Society for Microbial Ecology, Halifax, pp 181-192.

Benner, R., Biddanda, B., Black, B., McCarthy, M., 1997. Abundance, size distribution, and stable carbon and nitrogen isotopic compositions of marine organic matter isolated by tangential-flow ultrafiltration. Mar. Chem. 57, 243-263.

Benner, R., Amon, R.M.W., 2015. The size-reactivity continuum of major bioelements in the ocean. Annu. Rev. Mar. Sci. 7, 185-205.

Biddanda, B., Benner, R., 1997. Carbon, nitrogen, and carbohydrate fluxes during the production of particulate and dissolved organic matter by marine phytoplankton. Limnol. Oceanogr. 42, 506-518.

Broek, T., Guilderson, T.P., Bour, A.L., Yamaguchi, Y.T., McCarthy, M.D.,2016. Targeted isolation of refractory and semi-labile DOM or detailed molecular study: First results from the central north pacific subtropical gyre [abstract]. Ocean Sciences Meeting, 2016 Feb 21-26; New Orleans, LA. Abstract CT43A-06.

Bronk, D.A., See, J.H., Bradley, P., Killberg, L., 2007. DON as a source of bioavailable nitrogen for phytoplankton. Biogeosciences 4, 283-296.

Buesseler, K.O., Lamborg, C.H., Boyd, P.W., Lam, P.J., Trull, T.W., Bidigare, R.R., Bishop, J.K.B., Casciotti, K.L., Dehairs, F., Elskens, M., et. al., 2007. Revisiting carbon flux through the ocean's twilight zone. Science 316, 567-570.

Calleja M.Ll., Batista F., Peacock M., Kudela R., McCarthy M.D., 2013. Changes in compound specific $\delta^{15}N$ amino acid signatures and D/L ratios in marine dissolved organic matter induced by heterotrophic bacterial reworking. Mar. Chem. 149, 32-44.

Ciais, P., C. Sabine, G. Bala, L. Bopp, V. Brovkin, J. Canadell, A. Chhabra, R. DeFries, J. Galloway, M. Heimann, C. Jones, C. Le Quéré, R.B. Myneni, S. Piao and P. Thornton, 2013. Carbon and Other Biogeochemical Cycles, in: Stocker, T.F., D. Qin, G.-K. Plattner, M. Tignor, S.K. Allen, J. Boschung, A. Nauels, Y. Xia, V. Bex and P.M. Midgley (Eds.), Climate Change 2013: The Physical Science Basis. Contribution of Working Group I to the Fifth Assessment Report of the Intergovernmental Panel on Climate Change. Cambridge University Press, Cambridge, United Kingdom and New York, NY, USA.

Dauwe, B., Middelburg, J.J., Herman, P.M.J., Heip, C.H.R., 1999. Linking diagenetic alteration of amino acids and bulk organic matter reactivity. Limnol. Oceanogr. 44, 1809-1814.

Davis, J., Benner, R., 2005. Seasonal trends in the abundance, composition, and bioavailability of particulate and dissolved organic matter in the Chukchi/Beaufort Seas and western Canada Basin. Deep-Sea Res. II, 52, 3396-3410.

Décima, M., Landry, M.R., Popp, B.N., 2013. Environmental perturbation effects on baseline $\delta^{15}N$ values and zooplankton trophic flexibility in the southern California Current Ecosystem. Limnol. Oceanogr. 58, 624-634.

Dittmar, T., Fitznar, H.P., Kattner, G., 2001. Origin and biogeochemical cycling of organic nitrogen in the Eastern Arctic Ocean as evident from D- and L-amino acids. Geochim. Cosmochim. Ac. 65, 4103-4114.

Dittmar, T., Koch, B., Hertkorn, N., Kattner, G., 2008. A simple and efficient method for the solid phase extraction of dissolved organic matter (SPE-DOM) from seawater. Limnol. Oceanogr.-Meth. 6, 230-235.

Druffel, E.R.M., Williams, P.M., Bauer, J.E., Ertel, J.R., 1992. Cycling of dissolved and particulate organic matter in the open ocean. J. Geophys. Res. 97, 15639-15659.

Ducklow, H., 2000. Bacterial production and biomass in the oceans, in: Kirchman, D.L. (Ed.), Microbial Ecology of the Oceans. Wiley-Liss, New York , pp 85-120.

Eglinton, T.I., Repeta, D.J., 2006. Organic matter in the contemporary ocean, in: Elderfield, H (Ed.), Treatise on Geochemistry, Volume 6: The Oceans and Marine Geochemistry. Elsevier, Amsterdam, pp 145-180.

Flerus, R., Lechtenfeld, O.J., Koch, B.P., McCallister, S.L., Schmitt-Kopplin, P., Benner, R., Kaiser, K., Kattner, G., 2012. A molecular perspective on the ageing of marine dissolved organic matter. Biogeosciences 9, 1935-1955.

Guo, L., Santschi, P., Warnken, K.W., 1995. Dynamics of dissolved organic carbon (DOC) in oceanic environments. Limnol. Oceanogr. 40, 1392-1403.

Hansell, D.A., Carlson, C.A., Repeta, D.J., Schlitzer, R., 2009. Dissolved organic matter in the ocean: A controversy stimulates new insights. Oceanography 22, 202-211.

Hedges, J.I., 1992. Global biogeochemical cycles: Progress and problems. Mar. Chem. 39, 67-93.

Hedges, J.I., Eglinton, G., Hatcher, P.G., Kirchman, D.L., Arnosti, C., Derenne, S., Evershed, R.P., Kögel-Knabner, I., de Leeuw, J.W., Littke, R., Michaelis, W., Rullkötter, J., 2000. The molecularly-uncharacterized component of nonliving organic matter in natural environments. Org. Geochem. 31, 945-958.

Jiao, N., Herndl, G.J., Hansell, D.A., Benner, R., Kattner, G., Wilhelm, S.W., Kirchman, D.L., Weinbauer, M.G., Luo, T., Chen, F., Azam, F., 2010. Microbial production of recalcitrant dissolved organic matter: long-term carbon storage in the global ocean. Nat. Rev. Microbiol. 8, 593-599.

Kaiser, K., Benner, R., 2005. Hydrolysis-induced racemization of amino acids. Limonl. Oceanogr. Meth. 3, 318-325.

Kaiser, K., Benner, R., 2008. Major bacterial contribution to the ocean reservoir of detrital organic carbon and nitrogen. Limnol. Oceanogr. 53, 99-112.

Kaiser, K., Benner, R., 2009. Biochemical composition and size distribution of organic matter at the Pacific and Atlantic time series stations. Mar. Chem. 113, 63-77.

Kirchman, D.L., 2004. A primer on dissolved organic material and heterotrophic prokaryotes in the oceans, in: Follows, M., Oguz, T. (Eds.), The Ocean Carbon Cycle and Climate. Kluwer Academic Publishers, the Netherlands, pp 31-63.

Koch, B.P., Witt, M.R., Engbrodt, R., Dittmar, T., Kattner, G., 2005. Molecular formulae of marine and terrestrial dissolved organic matter detected by electrospray ionization Fourier transform ion cyclotron resonance mass spectrometry. Geochim. Cosmochim. Ac. 69, 3299-3308.

Kujawinski, E.B., 2011. The impact of microbial metabolism on marine dissolved organic matter. Annu. Rev. Mar. Sci. 3, 567-599.

Lechtenfeld, O.J., Hertkorn, N., Shen, Y., Witt, M., Benner, R., 2015. Marine sequestration of carbon in bacterial metabolites. Nat. Commun. 6:6711. (DOI: 10.1038/ncomms7711)

Lee C., Wakeham S.G., Hedges J.I., 2000. Composition and flux of particulate amino acids and chloropigments in equatorial pacific seawater and sediments. Deep Sea Res. 1, 47, 1535-1568.

Loh, A.N., Bauer, J.E., Druffel, E.R.M., 2004. Variable ageing and storage of dissolved organic components in the open ocean. Nature 430, 877-881.

Mao, J., Kong, X., Schmidt-Rohr, K., Pignatello, J.J., Perdue, E.M., 2010. Advanced solid-state NMR characterization of marine dissolved organic matter isolated using coupled reverse osmosis/electrodialysis method. Environ. Sci. Technol. 46, 5806-5814.

Martinez, J.S., Zhang, G.P., Holt, P.D., Jung, H.T., Carrano, C.J., Haygood, M.G., Butler, A., 2000. Self-assembling amphiphilic siderophores from marine bacteria. Science 287, 1245-1247.

McCarthy, M., Hedges, J., Benner, R., 1996. Major biochemical composition of dissolved high molecular weight organic matter in seawater. Mar. Chem. 55, 281-297.

McCarthy, M., Pratum, T., Hedges, J., Benner, R., 1997. Chemical composition of dissolved organic nitrogen in the ocean. Nature 390, 150-154.

McCarthy, M.D., Hedges, J.I., Benner, R., 1998. Major bacterial contribution to marine dissolved organic nitrogen. Science 281, 231-234.

McCarthy, M.D., Benner, R., Lee, C., Hedges, J.I., Fogel, M.L., 2004. Amino acid carbon isotopic fractionation patterns in oceanic dissolved organic matter: An

unaltered photoautotrophic source for dissolved organic nitrogen in the ocean? Mar. Chem. 92, 123-134.

McCarthy, M.D., Benner, R., Lee, C., Fogel, M.L., 2007. Amino acid nitrogen isotopic fractionation patterns as indicators of heterotrophy in plankton, particulate, and dissolved organic matter. Geochim. Cosmochim. Acta 71, 4727-4744.

McCarthy, M.D., Beaupré, S.R., Walker, B.D., Voparil, I., Guilderson, T.P.,Druffel, E.R.M., 2011. Chemosynthetic origin of ^{14}C-depleted dissolved organic matter in a ridge-flank hydrothermal system. Nat. Geosci. 4, 32-36.

Mitchell, J.B.O., Smith, J., 2003. D–amino acid residues in peptides and proteins. Proteins 50, 563-571.

Moore, C.M., Mills, M.M., Arrigo, K.R., Berman-Frank, I., Bopp, L., Boyd, P.W., Galbraith, E.D., Geider, R.J., Guieu, C., Jaccard, S.L., Jickells, T.D., La Roche, J., Lenton, T.M., Mahowald, N.M., Maranon, E., Marinov, I., Moore, J.K., Nakatsuka, T., Oschlies, A., Saito, M.A., Thingstad, T.F., Tsuda, A., Ulloa, O., 2013. Processes and patterns of oceanic nutrient limitation. Nat. Geosci. 6, 701-710.

Nagata, T., Kirchman, D.L., 1999. Bacterial mortality: A pathway for the formation of refractory DOM, in: Bell, C.R., Brylinsky, M., Johnson-Green, P. (Eds.), Microbial Biosystems: New Frontiers. Proceedings of the 8th International Symposium on Microbial Ecology. Atlantic Canada Society for Microbial Ecology, Halifax, pp 153-158.

Nagata, T., Meon, B., Kirchman, D.L., 2003. Microbial degradation of peptidoglycan in seawater. Limnol. Oceanogr. 48, 745-754.

Ogawa, H., Amagai, Y., Koike, I., Kaiser, K., Benner, R., 2001. Production of refractory dissolved organic matter by bacteria. Science 292, 917-920.

Pérez, M.T., Pausz, C., Herndl, G.J., 2003. Major shift in bacterioplankton utilization of enantiomeric amino acids between surface waters and the ocean's interior. Limnol. Oceanogr. 48, 755-763.

Raaijmakers, J.M., deBruijn, I., Nybroe, O., Ongena, M., 2010. Natural functions of lipopeptides from Bacillus and Pseudomonas: More than surfactants and antibiotics. FEMS Microbiol. Rev. 34, 1037-1062.

Radkov, A.D., Moe, L.A., 2014. Bacterial synthesis of D-amino acids. Appl. Microbiol. Biotechnol. 98, 5363-5374.

Repeta, D.J., 2015. Chemical characterization and cycling of dissolved organic matter, in: Hansell, D.A., Carlson, C.A. (Eds.), Biogeochemistry of Dissolved Organic Matter. Elsevier, Amsterdam, pp 21-63.

Roland, L.A., McCarthy, M.D., Peterson, T.D., Walker, B.D., 2009. A large-volume microfiltration system for isolating suspended particulate organic matter: Fabrication and assessment vs GFF filters in central North Pacific. Limnol. Oceanogr.-Meth. 7, 64-80.

Schliefer K.H., Kandler O., 1972. Peptidoglycan types of bacterial cell walls and their taxonomic implications. Bacteriol. Rev. 36, 407-477.

Silfer, J.A., Engel, M.H., Macko, S.A., Jumeau, E.J., 1991. Stable carbon isotope analysis of amino acid enantiomers by conventional isotope ratio mass spectrometry and combined gas chromatography/isotope ratio mass spectrometry. Anal. Chem. 63, 370-374.

Sipler, R.E., Bronk, D.A., 2015. Dynamics of dissolved organic nitrogen, in: Hansell, D.A., Carlson, C.A. (Eds.), Biogeochemistry of Dissolved Organic Matter. Elsevier, Amsterdam, pp 128-232.

Stuiver, M., Polach, H.A., 1977. Discussion: Reporting of ^{14}C data. Radiocarbon 9, 355-363.

Takano, Y., Kashiyama, Y., Ogawa, N.O., Chikaraishi, Y., Ohkouchi, N., 2010. Isolation and desalting with cation-exchange chromatography for compound-specific nitrogen isotope analysis of amino acids: Application to biogeochemical samples. Rapid Commun. Mass Sp. 24, 2317-2323.

Vogel, J.S., Southon, J.R., Nelson, D.E., Brown, T.A., 1984. Performance of catalytically condensed carbon for use in accelerator mass spectrometry. Nucl. Instrum. Meth. B 289-293.

Walker, B.D., Beaupre, S.R., Guilderson, T.P., Druffel, E.R.M., McCarthy, M.D., 2011. Large-volume ultrafiltration for the study of radiocarbon signatures and size vs. age relationships in marine dissolved organic matter. Geochim. Cosmochim. Ac. 75, 5187-5202.

Walker, B.D., McCarthy, M.D, 2012. Elemental and isotopic characterization of dissolved and particulate organic matter in a unique California upwelling system: Importance of size and composition in the export of labile material. Limnol. Oceanogr. 57, 1757-1774.

Walker, B.D., Guilderson, T.P., Okimura, K.M., Peacock, M.B., McCarthy, M.D., 2014. Radiocarbon signatures and size-age-composition relationships of major organic matter pools within a unique California upwelling system. Geochim. Cosmochim. Ac. 126, 1-17.

Walker, B.D., Beaupré, S.R., Guilderson, T.P., M.D. McCarthy, M.D., Druffel, E.R.M., 2016. Pacific carbon cycling constrained by organic matter size, age, and composition relationships. Nat. Geosci. 9, 888-891.

Woodward, F.I., 2007. Global primary production. Curr. Biol. 17, R269-R273.

Yamashita, Y., Tanoue, E., 2003. Distribution and alteration of amino acids in bulk DOM along a transect from bay to oceanic waters. Mar. Chem. 82, 145-160.

Ziolkowski, L.A., Druffel, E.R.M., 2010. Aged black carbon identified in marine dissolved organic carbon. Geophys. Res. Lett. 37, L16601.